Reprinted from Journal of the Optical Society of America B, Vol. 5, page 1503, July 1988

Optimization of two-photon-resonant four-wave mixing: application to 130.2-nm generation in mercury vapor

A. V. Smith, W. J. Alford, and G. R. Hadley

Sandia National Laboratories, Albuquerque, New Mexico 87185

Received September 18, 1987; accepted March 21, 1988

A detailed model of two-photon-resonant four-wave mixing that includes the consideration of efficiency-limiting processes is presented. The model provides a generally applicable systematic approach for maximizing conversion efficiencies for both exact and near two-photon resonance. For exact two-photon resonance, an interference effect limits efficiency to a value determined by ratios of nonlinear susceptibilities and input intensities. For near two-photon resonance, nonlinear refractive indices limit efficiencies unless input intensities are properly balanced. For the specific case of 130.2-nm generation in Hg, we examine a number of potential additional efficiency-limiting processes, including amplified spontaneous emission, stimulated Raman and hyper-Raman gain, parametric gain, linear absorption, and population transfer. We include isotopic effects and Gaussian-profile beams. From our analysis, we conclude that efficiencies of approximately 10% should be feasible by using collimated light beams in an energy-scalable system.

1. INTRODUCTION

The generation of coherent light at the atomic-oxygen resonance wavelength of 130.2 nm (76 795 cm^{-1}) has been achieved by using a variety of methods. For example, the sixth anti-Stokes shift of an ArF laser[1] in H_2 and four-wave mixing in Zn,[2] Mg,[3] Hg,[4] and Cd (Ref. 5) atomic vapors are all proven sources of light near 130 nm. However, the demonstrated optical conversion efficiencies are low. We propose here a four-wave-mixing technique that we believe will generate 130-nm light with an efficiency $\approx$10% in an energy-scalable system. This is a considerably higher mixing efficiency than is typically observed for four-wave mixing in gases. There is some precedent, however, in that efficiencies of several per cent have been demonstrated in a few cases by using picosecond-duration light pulses and focused geometries.[6] Also, Mahon and Tomkins[7] demonstrated 1% efficiencies for the generation of 125-nm light in Hg vapor by using 20-nsec pulses and a focused geometry.

Our proposed mixing scheme for 130-nm generation is shown in the Hg atomic-level diagram of Fig. 1. The Hg 7^1S level provides the two-photon-resonant enhancement. The frequencies ω_1 and ω_2 (39 212 and 24 716 cm^{-1} or 255.0 and 404.6 nm) are chosen to index match the process for collinear collimated beams in pure Hg vapor.[8] The nonlinear susceptibility is large[8] because the detuning from 6^3P_1 is 200 cm^{-1} and the detuning from 8^1P_1 is 68 cm^{-1}. This choice of frequencies is not unique. Index matching can be accomplished by tuning ω_1 slightly to the red of either the 6^1P_1 or the 6^3P_1 level, perhaps with the addition of a rare-gas buffer. We will discuss this possibility in more detail below.

The objective of this paper is to present as thorough an analysis as possible of the generation of 130-nm O_2 resonance light by using the mixing process shown in Fig. 1. In the course of this analysis we consider the broader question of optimizing (near) two-photon-resonant four-wave mixing processes in general. We discuss only unfocused mixing geometries because our applications require energy scalability and high optical quality for the output wave. For collimated geometries, energies can be scaled by expanding the beam radii. We will also show that high optical-beam quality can be achieved by using collimated beams. Additionally, the use of collimated beams avoids the necessity of understanding the nonlinear interactions at high intensities ($I > 10^8$ W/cm^2) encountered with focused beams and so permits more accurate modeling. Those processes that might limit conversion efficiencies in the case of 130-nm generation are given careful consideration. We will show that efficiencies equal to or greater than those demonstrated for focused geometries should be possible.

The organization of the paper is as follows. In Section 2 we consider the optimization of general (near) two-photon-resonant sum- or difference-frequency mixing processes, allowing for pump depletion and including all features intrinsic to two-photon-resonant mixing. This is an extension of earlier work by Kildal and Brueck[9] on optimizing two-photon-resonant third-harmonic generation. The principal extension here is that the intensities of the three input waves are independently adjustable. This permits more flexibility in optimizing mixing efficiency and leads to higher predicted efficiencies than in the case of third-harmonic generation.

In Section 3 we apply the optimization to the generation of 130.2-nm light by the process shown in Fig. 1 and incorporate features specific to this mixing process, such as ac-Stark shifts, amplified spontaneous emission (ASE) from the pumped two-photon-resonant level, Raman and hyper-Raman loss mechanisms, and parametric processes. These processes set limits on operating parameters and limit mixing efficiencies. The calculation details for the various limiting processes are presented in the appendixes. Section 4 contains a summary of our results and our conclusions.

0740-3224/88/071503-17$02.00

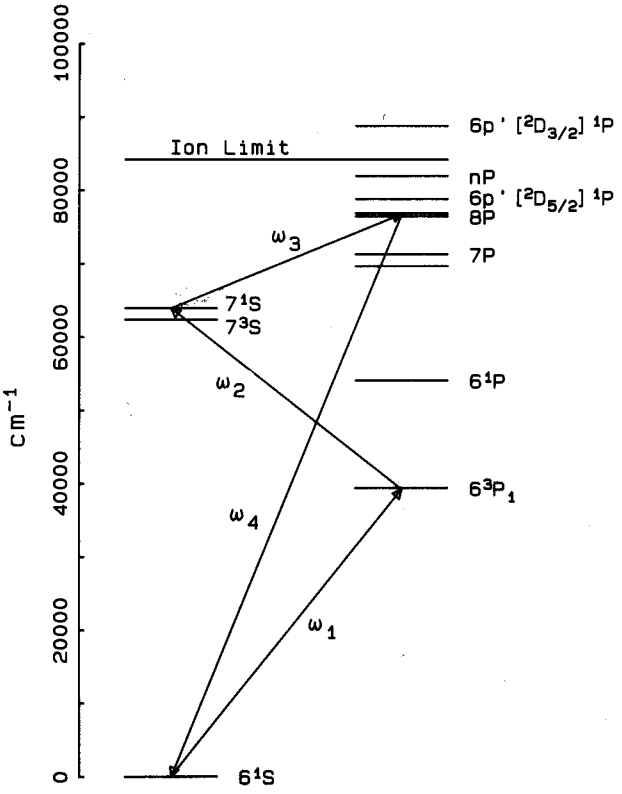

Fig. 1. Energy-level diagram of Hg showing proposed mixing process for generation of 130.2-nm light. Wavelengths one, two, and three are 255.0, 404.6, and 777.2 nm, respectively. Wave one is detuned by 200 cm^{-1} to the red of the 6^3P_1 level. Wave four is detuned by 68 cm^{-1} to the red of the 8^1P_1 level.

2. GENERAL TWO-PHOTON-RESONANT FOUR-WAVE MIXING

In this section we present and analyze the equations relating the third-order nonlinear interactions among the four mixing waves. These equations form a set of coupled differential equations that describe the evolution of the interacting waves and of population transfer in the medium. Because of the difficulty of obtaining analytical solutions to this set of equations, we resort to numerical integration. The results are presented first for the case of exact two-photon resonance and then for the case of near resonance. In this section we present results and observations valid in general for four-wave mixing near a two-photon resonance. For concreteness, we use the parameters appropriate for the generation of 130.2-nm light by mixing in Hg unless otherwise noted.

In the mixing equations only the third- or lowest-order nonlinearity is considered, and only those terms enhanced by the two-photon resonance are retained. We use steady-state nonlinear susceptibilities. Only sum-frequency generation is treated. The equations for difference-frequency mixing are slightly different and can be found in Ref. 10. Under these conditions, the following four equations[10] relate the evolution of the four waves of frequency $\omega_1 - \omega_4$:

$$\frac{dA_1}{dz} - \frac{i}{4\pi\omega_1}\nabla_\perp{}^2 A_1 = iCN\frac{\omega_1}{n_1}S(\Delta_i)[\chi_{12}{}^*\chi_{34}A_4A_3{}^*A_2{}^* \times \exp(i\Delta kz) + |\chi_{12}|^2A_2|A_2|^2], \quad (1)$$

$$\frac{dA_2}{dz} - \frac{i}{4\pi\omega_2}\nabla_\perp{}^2 A_2 = iCN\frac{\omega_2}{n_2}S(\Delta_i)[\chi_{12}{}^*\chi_{34}A_4A_3{}^*A_1{}^* \times \exp(i\Delta kz) + |\chi_{12}|^2A_2|A_1|^2], \quad (2)$$

$$\frac{dA_3}{dz} - \frac{i}{4\pi\omega_3}\nabla_\perp{}^2 A_3 = iCN\frac{\omega_3}{n_3}S^*(\Delta_i)[\chi_{12}{}^*\chi_{34}A_4A_2{}^*A_1{}^* \times \exp(i\Delta kz) + |\chi_{34}|^2A_3|A_4|^2], \quad (3)$$

$$\frac{dA_4}{dz} - \frac{i}{4\pi\omega_4}\nabla_\perp{}^2 A_4 = iCN\frac{\omega_4}{n_4}S(\Delta_i)[\chi_{12}\chi_{34}{}^*A_1A_2A_3 \times \exp(-i\Delta kz) + |\chi_{34}|^2A_4|A_3|^2]. \quad (4)$$

Here A_i is the complex electric-field amplitude at frequency ω_i measured in statvolts per centimeter, $C = \pi^2(ea_0)^4/(hc)^3 = 5.23 \times 10^{-23}$ cm^3/erg, N is the atomic density in inverse cubic centimeters, ω is in inverse centimeters, n are the refractive indices in the mixing medium, Δk is the low-intensity index mismatch $(k_4 - k_1 - k_2 - k_3)$ in inverse centimeters, $S(\Delta_i)$ is a line-shape function describing the two-photon resonance as defined below, and χ are partial susceptibilities defined by

$$\chi_{12} = \sum_m \left[\frac{\langle i|\mathbf{d}\cdot\hat{e}_2|m\rangle\langle m|\mathbf{d}\cdot\hat{e}_1|g\rangle}{\omega_m - \omega_1} + \frac{\langle i|\mathbf{d}\cdot\hat{e}_1|m\rangle\langle m|\mathbf{d}\cdot\hat{e}_2|g\rangle}{\omega_m - \omega_2}\right], \quad (5)$$

$$\chi_{34} = \sum_m \left[\frac{\langle i|\mathbf{d}\cdot\hat{e}_3|m\rangle\langle m|\mathbf{d}\cdot\hat{e}_4|g\rangle}{\omega_m - \omega_4} + \frac{\langle i|\mathbf{d}\cdot\hat{e}_4|m\rangle\langle m|\mathbf{d}\cdot\hat{e}_3|g\rangle}{\omega_m - \omega_3}\right], \quad (6)$$

$$S(\Delta_i) = \frac{1}{w\pi^{1/2}}\int_{-\infty}^{+\infty}\frac{\exp(-x^2)}{x - \zeta}\,dx = Z(\zeta)/w, \quad (7)$$

$$\zeta = (\omega_1 + \omega_2 - \omega_i + i\Gamma_i)/w = (\Delta_i + i\Gamma_i)/w, \quad (8)$$

$$w = \omega_i(2kT/mc^2)^{1/2} = \Delta\omega_D/2(\ln 2)^{1/2}. \quad (9)$$

The units of χ are $(ea_0)^2/cm^{-1}$. $\hat{e}_j$ is the unit polarization vector of wave ω_j, and the matrix elements in the numerators are of electric-dipole operators. $\Delta\omega_D$ is the Doppler width (FWHM) in inverse centimeters, and $S(\Delta_i)$ is a Doppler-averaged Lorentzian (of half-width Γ_i) with units of centimeters. Δ_i is $\omega_1 + \omega_2 - \omega_i$, where ω_i is the energy of the two-photon-resonant level and Z is the plasma dispersion function.[11] The relationship of χ and $S(\Delta_i)$ to the usual definition of the third-order susceptibility is

$$\chi^{(3)}(-\omega_4;\omega_1,\omega_2,\omega_3) = 8.87 \times 10^{-25}S(\Delta_i)\chi_{12}\chi_{34}{}^*, \quad (10)$$

where $\chi^{(3)}$ has units of cm^6/erg.

Consider Eq. (1). It has two terms on the right-hand side of the equal sign. The first term is proportional to the field amplitudes of the other three waves and may be associated with a four-wave-mixing process. The second term is proportional to A_1 and $|A_2|^2$ and thus can be thought of as a nonlinear refractive-index term. For exact two-photon res-

onance, this term is pure imaginary because the real part of $S(\Delta_i)$ vanishes. This leads to two-photon absorption of waves one and two [note that Eq. (2) has a similar second term]. For nonzero detunings, $S(\Delta_i)$ has a sizable real part, and the associated real part of the second term describes an intensity-dependent refractive index. The first terms on the right-hand sides of Eqs. (2)–(4) can similarly be associated with four-wave mixing; the second terms describe two-photon absorption in the case of Eq. (2) or Raman scattering for Eqs. (3) and (4).

The population of the two-photon-resonant state i as a function of time is determined from the rate equation

$$\frac{\partial N_i}{\partial t} = 16\hbar C S''(\Delta_i)|\chi_{12}A_1A_2 + \chi_{34}A_3^*A_4 \exp(i\Delta kz)|^2, \quad (11)$$

where C is the same as in Eqs. (1)–(4) and S'' is the imaginary part of S. The first term is associated with two-photon absorption from waves one and two, and the second term is associated with the Raman process involving waves three and four. Because the amplitudes for these two processes add (rather than their intensities), interference effects can strongly influence the population of the two-photon-resonant state. Such effects will be discussed in detail later in this section.

In our numerical solution of Eqs. (1)–(4) we assume cylindrical symmetry and discretize the equations on a spatially varying mesh. We then propagate each of the four beams through the nonlinear mixing medium by using a well-known tridiagonal algorithm.[12] The first three beams are given initial spatial profiles (plane wave or Gaussian) that may change as the beams propagate owing to a number of effects, including nonlinear refractive indices, pump-wave depletion, and diffraction. The fourth wave is initially given a zero amplitude, and thus its spatial profile is determined by Eqs. (1)–(4) as the propagation proceeds. In this way we are able to study beam quality as well as total conversion efficiency. This is an important feature of the solution method, for we have found that certain parameter combinations that yield high conversion efficiencies do so at the expense of beam quality.

In the discussion that follows we will assume that the input waves are infinite-extent plane waves in order to emphasize the essential aspects of the mixing process. Thus the transverse derivative terms are set to zero. Later, when we apply the modeling to the specific case of 130.2-nm generation with Gaussian beams in Hg, we will include diffractive effects, and the spatial-intensity profiles will be calculated at each point in the mixing medium.

Although we will model the conversion process by assuming specific values for the susceptibilities, detunings, etc., the results can be easily extended to other sets of parameters by using simple scaling properties, which we will point out.

A. On Resonance

First we consider the case of exact two-photon resonance with a single Doppler-broadened line with $\Delta\omega_D = 0.067$ cm^{-1}. The wavelengths of waves one through four are 255.0, 404.6, 777.2, and 130.2 nm, respectively. They are appropriate for the mixing process discussed in the latter part of this paper. Another choice of wavelengths will give somewhat different results, but the qualitative features that we emphasize here will not be affected. Likewise, the product of χ_{12} and χ_{34} is 3.6×10^{-7} $([ea_0]^2/cm^{-1})^2$, as is appropriate for 130.2-nm generation in Hg. However, the ratio of χ_{12}/χ_{34} will be permitted to vary. In practice, the choice of sum frequency and two-photon-resonant state will establish the value of χ_{34}; the value of χ_{12} can be varied by selecting frequencies one and two consistent with index matching.

As an example of our solution technique, Fig. 2 shows the result for a 1-nsec square pulse propagating through a mixing medium with a density of 2×10^{17} cm^{-3} for $\chi_{12}/\chi_{34} = 0.725$. We plot here the intensities of the four waves and the two-photon-resonant-state population as a function of position through the mixing cell. We have assumed $\Delta k = 0$ and input intensities of 3.05, 1.92, and 1.00 MW/cm^2 for waves one, two, and three, respectively, i.e., equal photon fluxes. The striking feature of Fig. 2 is the sharp saturation of the mixing after a distance of approximately 20 cm. Once saturation is reached, no further energy exchange occurs between the waves, and population transfer to the two-photon-resonant level ceases. This is due to a destructive interference between two pathways from the ground level to the

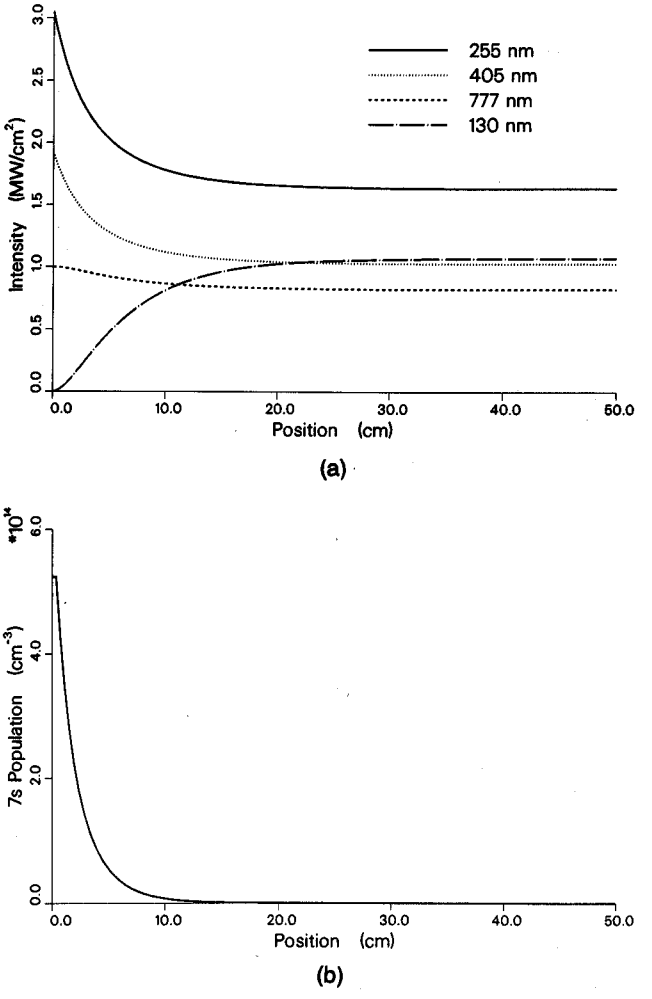

Fig. 2. (a) Calculated intensities in waves one (solid line), two (dotted line), three (dashed line), and four (dashed–dotted line) as a function of position in the mixing cell. Assumes plane waves, single isotope, 0.067-cm^{-1} Doppler width two-photon resonance, $N = 2 \times 10^{17}$ cm^{-3}, no ASE, $\chi_{12} = 5.1 \times 10^{-4}$, $\chi_{34} = 7.0 \times 10^{-4}$. (b) Calculated 7^1S population density versus position along the mixing cell at the end of 1-nsec pulse for the same conditions as in (a).

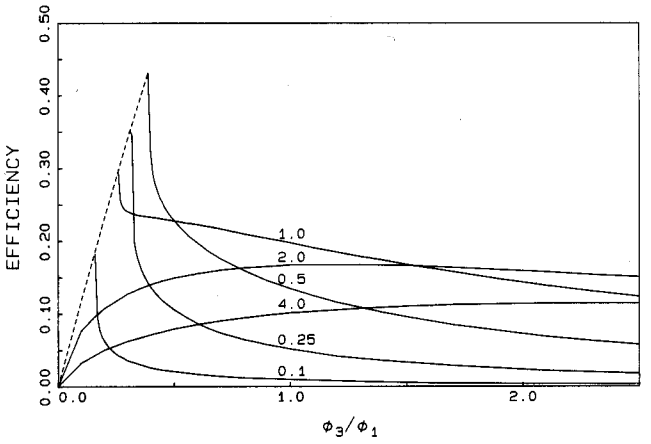

Fig. 3. Maximum sum-frequency conversion efficiency as a function of photon-flux ratio ϕ_3/ϕ_1 for ratios of χ_{12}/χ_{34} from 0.1 to 4.0 ($\chi_{12}\chi_{34} = 3.5 \times 10^{-7}$ $[ea_0]^4$ cm^2) for exact resonance and plane waves. The dashed line is explained in the text. The input frequencies are those appropriate for 130.2-nm generation.

two-photon-resonant level that have equal but opposite amplitudes when

$$\chi_{12}A_1A_2 = -\chi_{34}A_3^*A_4 \exp(i\Delta kz). \tag{12}$$

When this condition is satisfied, the right-hand sides of Eqs. (1)–(4) and Eq. (11) are equal to zero. This destructive interference is a general feature of exact-resonance mixing processes and has been extensively discussed in connection with two-photon-resonant sum- and difference-frequency mixing[9,13] and three-photon-resonant sum-frequency mixing.[14]

The interference imposes a fundamental limit on mixing efficiency for exact two-photon resonance. To find the limiting efficiency for a particular value of the ratio χ_{12}/χ_{34}, it is necessary to determine the optimum balance of input intensities. Photons are lost to two-photon absorption as well as in conversion to sum-frequency light, so that although the balance described in Eq. (12) holds at saturation, the optimum input fluxes must be determined empirically. We expect (and have verified) that the photon fluxes in waves one and two should be equal because all the nonlinear processes lead to absorption or emission of equal numbers of photons in these waves (we neglect linear absorption of the light). Therefore we set $\phi_1 = \phi_2$ (where ϕ_i is the input photon flux in wave i) and vary ϕ_3/ϕ_1 to find the optimum photon-flux ratio.

Figure 3 shows a plot of mixing efficiency (defined as the energy emitted in wave four divided by the sum of the energies incident into waves one, two, and three) as a function of flux ratio ϕ_3/ϕ_1 for various values of χ_{12}/χ_{34}. The dashed line at low flux ratios indicates total absorption of input wave three before saturation due to interference can occur. The plotted efficiency is that at the point of complete ω_3 absorption (dashed line) or the saturated value (solid lines). In the region of the dashed line, after wave three has been completely absorbed, waves one, two, and three grow at the expense of wave four so that the actual output efficiency would fall somewhere below the dashed line. The peak values of efficiency that occur at the cusps adjacent to the dashed line for $\chi_{12}/\chi_{34} < 1$ correspond to the situation in which wave three is almost completely depleted in the cell. According to Eq. (12), this permits a high intensity in wave four.

The general pattern in which the maximum efficiency for large (≥ 2) values of χ_{12}/χ_{34} occurs at large (≥ 1) values of ϕ_3/ϕ_1 can be understood in terms of a balance between loss of energy to the medium through two-photon absorption and saturation due to the interference. For large values of χ_{12}/χ_{34}, two-photon absorption dominates, and efficiency is maximized by making wave three intense so that saturation occurs in a short distance, thus minimizing loss to the medium. In the other extreme of a small χ ratio, the maximum efficiency occurs for small (<1) values of ϕ_3/ϕ_1, as suggested by Eq. (12).

The high efficiencies close to the cusps in Fig. 3 are unlikely to be of practical value because they occur in regions where the slope of the efficiency with respect to the flux ratio is large. Any variation in ϕ_3/ϕ_1 would be magnified greatly in wave four, leading to severe wave distortions. Achieving the efficiencies calculated at the cusps also requires relatively large values of NL (the product of the interaction length and the medium density) because of the low intensity of wave three. For values of NL smaller than that of Fig. 3, the cusps are rounded off, as Fig. 4 shows for the case $\chi_{12}/\chi_{34} = 0.725$.

We have shown in Figs. 3 and 4 that for each value of NL and χ_{12}/χ_{34} there is a maximum efficiency obtainable by adjusting the input intensity of wave three relative to the input intensities of waves one and two, i.e., the value of ϕ_3/ϕ_1. In Fig. 5 these efficiency maxima are plotted as a function of χ_{12}/χ_{34} for three values of NL. The curve for large NL has a kink in the region of $\chi_{12}/\chi_{34} = 1$ because there are two local maxima in the plots of efficiency versus ϕ_3/ϕ_1. One occurs at the cusp, and another occurs at larger values of ϕ_3/ϕ_1. The kink occurs at the point of transition where the second maximum becomes the larger of the two. As these plots show, when NL is reduced, the maximum efficiency decreases from 45 to 22% over the range shown, but the optimum χ_{12}/χ_{34} value remains at approximately 0.5–0.7. The values of ϕ_3/ϕ_1 associated with the optimized efficiencies of Fig. 5 are plotted in Fig. 6. Generally, as the χ ratio

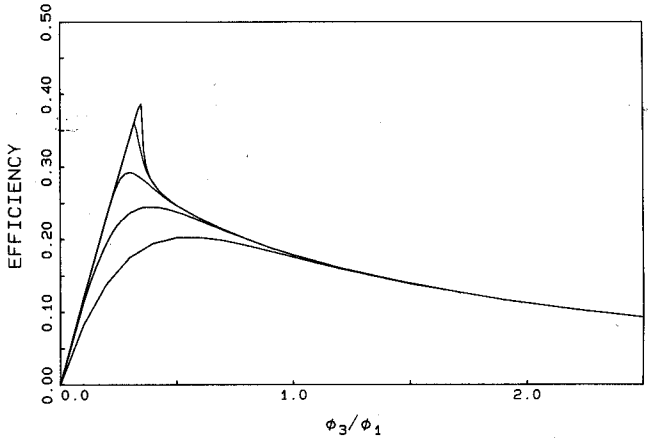

Fig. 4. On-resonance sum-frequency conversion efficiency as a function of photon-flux ratio ϕ_3/ϕ_1 for $\chi_{12} = 5.1 \times 10^{-4}$, $\chi_{34} = 7.0 \times 10^{-4}$ for various values of NL. From top to bottom, $NL = 8.0 \times 10^{19}$, 4.0×10^{19}, 2.0×10^{19}, 1.0×10^{19}, 0.5×10^{19} cm^{-2}. $I_1 = 3.1$ MW/cm^2, $I_2 = 1.9$ MW/cm^2, $\Delta_{7S} = 0$, single isotope.

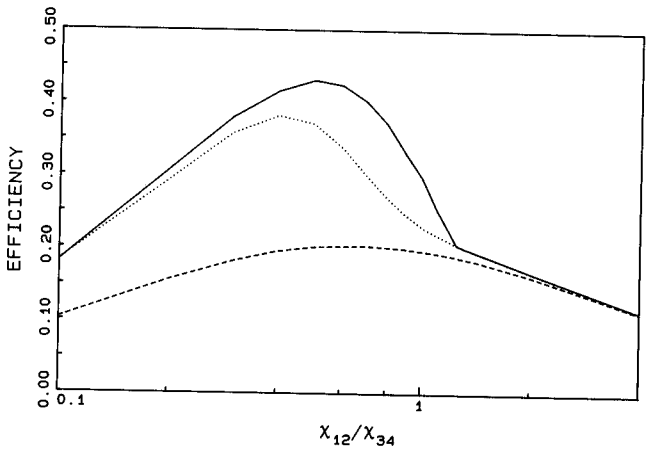

Fig. 5. Efficiency of sum-frequency generation optimized by adjusting ϕ_3/ϕ_1 as a function of χ_{12}/χ_{34} for (top to bottom) $NL = 3 \times 10^{20}$, 2×10^{19}, 5×10^{18}. $I_1 = 3.1$ MW/cm^2, $I_2 = 1.9$ MW/cm^2, $\chi_{12}\chi_{34} = 3.5 \times 10^{-7}$.

increases, the ϕ ratio does also with a slope of approximately 0.7 for the set of wavelengths considered here.

Although we have used specific values of number density N, resonance line-shape factor S, interaction length Z, input intensities I, and susceptibility χ ($\chi = \chi_{12}\chi_{34}$), the efficiency for one set of parameters χ, N, Z, I, and S is the same for other values so long as the ratios χ_{12}/χ_{34} and ϕ_3/ϕ_1 are maintained and the product χ^2NZIS is unchanged. This can be seen from the form of Eqs. (1)–(4) and has been verified by numerical integration. The sign of χ does not matter. The scaling is of course limited in scope because at some point competing processes, such as population transfer and multiphoton ionization, will become important. We will discuss these limiting processes below.

In principle, it is possible to exceed the conversion-efficiency limit imposed by the interference effect by using multiple mixing cells. If the sum-frequency waves are picked off between cells and then coherently recombined, the resulting efficiency is not limited by interference. In practice this would be technically difficult for 130-nm light, and we will asume that only one cell is used. Of course, if a spatially coherent wave at the sum frequency is not required, use of multiple cells may be a practical way of achieving higher efficiency.

In summary, for the case of exact two-photon resonance, a destructive-interference effect limits conversion efficiencies to well below 100%. The limit is set by the ratio of χ_{12}/χ_{34} and is achieved only by adjusting the ratio of input fluxes ϕ_3/ϕ_1 to an optimum value. The best efficiencies are possible for $\chi_{12}/\chi_{34} \approx 0.5$ and $\phi_3/\phi_1 \approx 0.5$. Efficiencies as great as 40% are predicted, and, for sufficiently large values of χ^2NZIS, efficiencies greater than 10% should be possible over a fairly broad range of the χ ratio. For choices of wavelengths different from those used here, these numbers will change somewhat. However, the general principle of maximizing mixing efficiency by balancing two-photon absorption against the negative interference effect is valid for any two-photon-resonant four-wave-mixing process.

B. Off Resonance

Thus far we have considered only exact two-photon resonance for which interference among the waves limits the efficiency. Perhaps by detuning slightly (a few Doppler widths) from the two-photon resonance, this limitation can be overcome. In this case the imaginary part of the nonlinear refractive-index terms in Eqs. (1)–(4) are small, so two-photon absorption and Raman scattering do not lead to an exchange of energy between the waves or to population transfer; hence the interference disappears. On the other hand, the real part of the nonlinear refractive indices associated with the two-photon resonance will be quite large. This will alter the relative phases of the four waves as they travel through the cell and will introduce a nonlinear contribution $\Delta k_{nl}(z)$ to the phase mismatch. This might limit mixing efficiency for off-resonance mixing.

The nonlinear refractive indices of waves one through four, given by the second term on the right-hand side in Eqs. (1)–(4), have the form

$$n_{nl}(\omega_1) \sim I_2|\chi_{12}|^2 S(\Delta_i). \tag{13}$$

Thus, if we tune slightly to the red (blue) side of the two-photon resonance, there will be a positive (negative) contribution to the refractive index of each wave. Because $\Delta k_{nl} = k_{nl}(\omega_4) - k_{nl}(\omega_1) - k_{nl}(\omega_2) - k_{nl}(\omega_3)$, if the value of $k_{nl}(\omega_4)$ is large enough to offset the other three k_{nl}, Δk_{nl} could be close to zero. $k_{nl}(\omega_4)$ is proportional to I_3, $k_{nl}(\omega_1)$ is proportional to I_2, and $k_{nl}(\omega_2)$ is proportional to I_1. Thus, for fixed intensities of waves one and two, it is possible to pick a value of I_3 that makes $\Delta k_{nl} = 0$. So, obviously, Δk_{nl} can be set to zero at the input window by adjusting the ratio ϕ_3/ϕ_1 (we assume that $\phi_1/\phi_2 = 1$). Because of the mixing process, however, the four waves change intensity as they pass through the mixing cell, so the question becomes whether it is possible to keep Δk_{nl} sufficiently small throughout the cell to permit high mixing efficiencies. Figure 7 shows plots of mixing efficiency versus cell length computed for various values of the photon-flux ratio ϕ_3/ϕ_1. For a ratio of 1.4, Δk_{nl} is quite small throughout the cell, and a mixing efficiency of 85% is theoretically possible.

It is also possible to compensate for the nonlinear mismatch for Δk_{nl} by fixing the photon-flux ratio and adjusting the linear mismatch Δk. In practice, Δk can often be adjusted by adding a buffer gas with the desired dispersion. For the χ ratio of 0.725, for example, we find that efficiencies

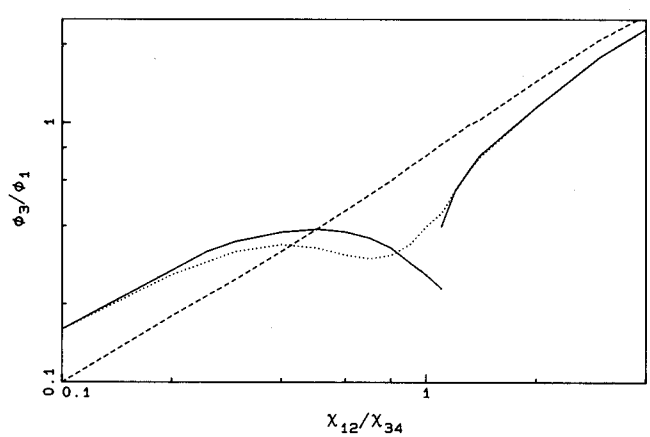

Fig. 6. Flux ratio needed for optimum efficiency of Fig. 5 as a function of χ_{12}/χ_{34} for $NL = 3 \times 10^{20}$ (solid line), 2×10^{19} (dotted line), 5×10^{18} (dashed line), $\chi_{12}\chi_{34} = 3.5 \times 10^{-8}$.

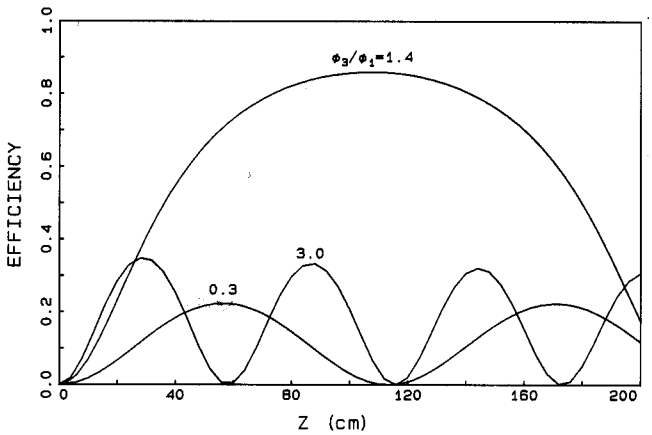

Fig. 7. Efficiency of 130.2-nm generation for off-resonant mixing as a function of position in the mixing cell for $\phi_3/\phi_1 = 0.3, 1.4, 3.0$: $I_1 = 3.1\ \mathrm{MW/cm^2}$, $I_2 = 1.9\ \mathrm{MW/cm^2}$, $\Delta_{7S} = 0.2\ \mathrm{cm^{-1}}$, $N = 4 \times 10^{17}\ \mathrm{cm^{-3}}$, $\Delta k = 0$.

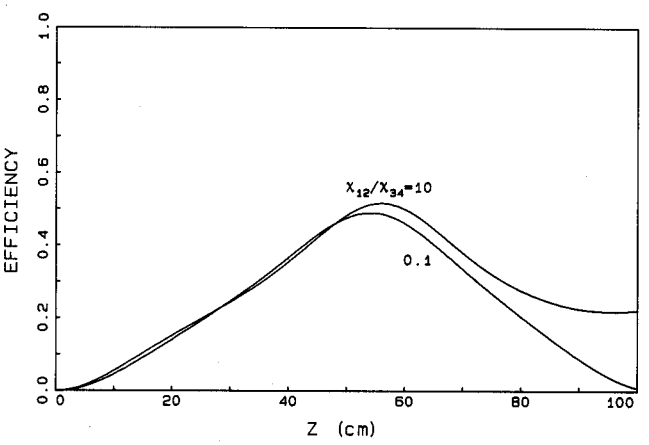

Fig. 8. Sum-frequency mixing efficiency for χ ratios of 0.1 and 10 optimized by adjusting both Δk and ϕ_3/ϕ_1.

exceeding 70% can be achieved for $0.67 < \phi_3/\phi_1 < 3$ by adjusting Δk. To achieve efficiencies approaching 100%, it is necessary to set $\phi_3/\phi_1 = 1$ and adjust Δk. Using this approach, we have calculated theoretical mixing efficiencies of 97%. These are not likely to be approached in practice because such high efficiency requires a long mixing length.

As may be seen from relation (13), the nonlinear refractive indices depend on the values of χ_{12} and χ_{34} as well as on the intensities. We showed that for $\chi_{12}/\chi_{34} = 0.725$, Δk_{nl} can be compensated for quite well. For other χ ratios, we find that for ratios near unity ($0.3 < \chi_{12}/\chi_{34} < 3$), good balance can be achieved. For ratios far from unity ($\chi_{12}/\chi_{34} = 10$ or 0.1, for example), only a partial balance can be achieved. Figure 8 shows an example for $\chi_{12}/\chi_{34} = 0.1$ and 10. The best efficiency predicted in either case is approximately 50% compared with the 97% noted above. For these cases it is necessary to vary Δk to obtain the best balance at a flux ratio near one. For example, for a χ ratio of 0.1, the best Δk is $+0.12\ \mathrm{cm^{-1}}$, and for a ratio of 10 it is $-0.35\ \mathrm{cm^{-1}}$ for the conditions of Fig. 8.

The calculations above are for plane waves. For Gaussian beams the intensities and thus the nonlinear refractive indices vary across the beam. Because we must be concerned with the phase profile of the sum-frequency wave, we have computed the phases of the waves at the exit window. We find that for on-axis intensities and other conditions the same as in Fig. 7, there is only a small ($<\lambda$) distortion of the phase front when the nonlinear mismatch is compensated for. The distortion is close to parabolic and thus should be readily correctable by using spherical optics.

The curves shown in Figs. 7 and 8 can be used to predict performance for other values of detuning, intensities, interaction lengths, and number densities by a simple scaling relation. For other values of detuning from resonance Δ_i, number density N, intensity of the input waves I, susceptibilities χ_{12} and χ_{34}, and interaction length Z, the efficiency plotted in Fig. 7 or 8 at the same value for $\chi^2 NZIS(\Delta_i)$ is still valid so long as the detuning is greater than approximately two Doppler widths and so long as the values of $\Delta k/N$ and χ_{12}/χ_{34} are unchanged. This scaling has been verified in our calculations over reasonable ranges of the parameters.

These results demonstrate that the limitation on efficiency imposed by the interference effect for on-resonance mixing can be overcome by tuning off resonance. For χ ratios near unity, nearly 100% conversion efficiency can be achieved. High-efficiency mixing requires careful adjustment of Δk and flux ratios to balance the effects of the intensity-dependent refractive indices.

3. GENERATION OF 130.2-nm LIGHT IN MERCURY

This section is devoted to developing a realistic model of 130.2-nm light generation by mixing in Hg. As in Section 2 we examine the two cases of on-resonance and off-resonance mixing separately. In addition to the efficiency-limiting effects discussed in Section 2, we consider other competing nonlinear-optical processes that may impose further limits on mixing efficiencies. We also discuss limits on Hg density, cell length, and input intensities, and we examine the sensitivity of mixing efficiency to probable variations in photon-flux ratios and changes in Δk.

The calculations will be based on our earlier measurements of Hg oscillator strengths and nonlinear susceptibilities.[15] The wavelengths of waves one, two, and three are 255.0, 404.6, and 777.2 nm, respectively. They are chosen to be two-photon resonant with the 7^1S level of Hg (see Fig. 1) and to index match sum-frequency generation of 130.2-nm light for unfocused, collinear input waves. The detuning from 8^1P is $68\ \mathrm{cm^{-1}}$, and detuning from 6^3P_1 is $200\ \mathrm{cm^{-1}}$. The partial susceptibilities are known to an accuracy of $\approx$20% and are $\chi_{12} = 5.1 \times 10^{-4}$ and $\chi_{34} = 7.0 \times 10^{-4}$ ($[ea_0]^2/\mathrm{cm^{-1}}$) for the wavelengths used here. Thus the product $\chi_{12}\chi_{34}$ and the wavelengths are those used in Section 2. The value of χ_{12}/χ_{34} is 0.72, which is close to the optimum value appearing in Fig. 5.

This set of wavelengths is preferred because of the near-optimal χ ratio and also because these wavelengths are relatively easy to generate by using pulsed lasers and standard frequency-conversion techniques in crystals. Other choices of wavelengths are possible. Wave one could be tuned closer to the 6^3P_1 level and index matched by adding a positively dispersive buffer gas. (Note that the use of many Torr of buffer gas such as Kr for index matching would probably lead to unacceptable absorption at 130.2 nm.) Similarly, wave one could be tuned to the red of the 6^1P level. Index

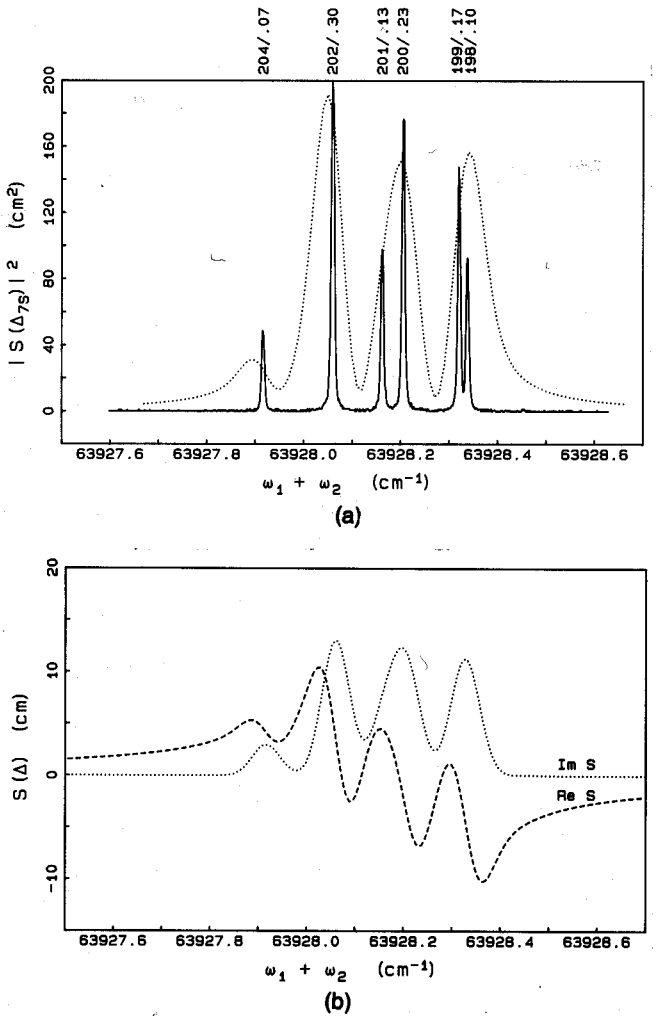

Fig. 9. (a) Isotope structure of the 6^1S–7^1S transition of Hg with natural isotopic abundances. The solid line is a measured Doppler-free fluorescence spectrum, and the dotted line is a computed curve of $|\langle S(7S)\rangle_{\text{Doppler}}|^2$. Labels at the top are isotopic mass/abundance. The wavelength scale is accurate to 0.01 cm^{-1}. (b) Computed real and imaginary values of $S(\Delta_{7S})$ for natural isotopic abundances.

matching in that case requires that the wavelength for ω_1 be 206 nm for pure Hg or shorter (down to the resonance at 184.9 nm) for index matching with buffer gas. ArF lases in this region at 193 nm and may also be of practical interest. The wavelength set would be 193, 825, and 777 nm. The χ ratio for these wavelengths is 2.2, so on-resonance mixing efficiencies of 18% are still possible according to Fig. 5. Index matching could be achieved by crossing beams or by adding a positively dispersive buffer gas. This case will not be specifically analyzed here; however, it should be qualitatively similar to the case described.

Before considering the details of the modeling, we note that Hg has seven abundant isotopes. The isotope shifts for the 6^1S–7^1S transition, shown in Fig. 9(a) for natural abundance Hg, are comparable with the Doppler width. The solid line in Fig. 9(a) was measured by using Doppler-free excitation by counterpropagating beams and fluorescence detection.[16] The labels at the top of the figure indicate the isotopic mass/abundance associated with each spectral peak. The dotted line is the corresponding calculated Doppler-broadened spectrum for sum-frequency mixing (proportional to $|S(\Delta_{7S})|^2$) as a function of $\omega_1 + \omega_2$. Figure 9(b) shows the real and imaginary parts of $S(\Delta_{7S})$. $|S(\Delta_{7S})|$ has a maximum value of 44 cm for a single isotope and 14 cm for natural abundance Hg. Although Hg is available[17] with various isotopes enriched, we will assume natural abundances unless stated otherwise.

To predict mixing efficiencies it is necessary to define reasonable limits for Z (the length of the mixing cell), N (the Hg density), and I (the input intensities). Details of the calculations on which we base our choices of these parameters are presented in Appendix A. Here we simply list the processes that we have considered and state the inferred limits for each quantity. The maximum allowed intensities are set by ac-Stark shifts at 15, 10, and 5 MW/cm^2 for waves one, two, and three, respectively. Consideration of beam divergence and practicality limits the cell length to 100 cm or less. A maximum Hg density of 2×10^{17} cm^{-3} is chosen to provide an adequate index-matched bandwidth and to keep absorption of the various light waves to acceptable levels. These are general limits. For specific mixing conditions, more-restrictive limits will apply.

In addition to the limits on efficiency imposed by interference and the allowed ranges of N, Z, and I, several competing or parasitic nonlinear processes diagrammed in Fig. 10 may also limit mixing efficiencies. For on-resonance mixing, these include ASE, parametric mixing, photoionization, and the effects of population transfer on index matching. For off-resonance mixing, Raman and hyper-Raman scattering may be important. Although each of these effects is dis-

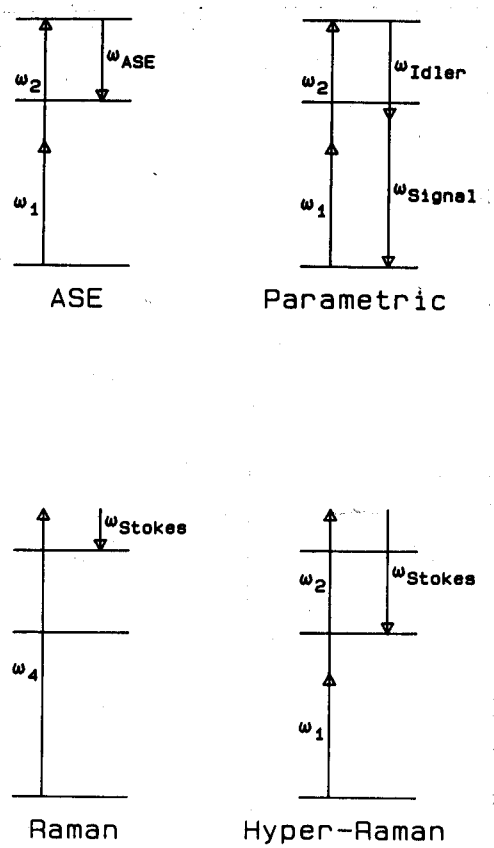

Fig. 10. Diagram of processes that can limit mixing efficiencies.

cussed in detail in the appendixes, we will briefly describe them here.

ASE (Fig. 10) involves emission from the two-photon-resonant 7^1S level to the $6^{1,3}P_1$ levels. The amplified light can build to intensities that power broaden the 7^1S–$6P_1$ ASE transitions. This modifies the 7^1S state and hence the 6^1S–7^1S two-photon transition. As a result, the effective value of $|S(\Delta_{7S})|$ is reduced. Parametric mixing (Fig. 10) can lead to exponential gain of new waves. This can reduce mixing efficiency by depleting the mixing waves or by creating destructive-interference effects similar to those discussed in Section 2 in connection with sum-frequency mixing. The Raman and hyper-Raman processes (Fig. 10) produce exponential growth of Stokes waves. If the gain is sufficient, the mixing waves could be depleted, resulting in reduced mixing efficiency. Photoionization or population transfer to the 7^1S and $6P$ levels might also change the refractive indices enough to destroy the index matching that is required for high efficiencies.

In this section we present an analysis of the mixing process, including all the limitations listed above, as well as a full treatment of the effects of nonplanar input waves. We will consider three cases: on-resonance mixing with single and with multiple isotopes and off-resonance mixing with multiple isotopes. We will also show that the case of off-resonance mixing for a single isotope is less efficient than off-resonance mixing with multiple isotopes.

A. On-Resonance Mixing

For a single isotope the term on resonance indicates that $\omega_1 + \omega_2$ is exactly resonant with the 6^1S–7^1S transition. Because the isotope shifts are quite large, for multiple isotopes this can be satisfied only for one particular isotope at a time. Thus, for multiple isotopes, both on- and off-resonance processes can occur simultaneously. In this case we use the term on-resonance mixing to indicate tuning to the dominant mass-202 resonance. We will reserve the term off-resonance mixing to indicate detuning by several Doppler widths from any of the isotopes. We discuss on-resonance mixing first for a single isotope and then for multiple isotopes, because the limiting processes can be different for the two situations.

1. *Single Isotope*

We begin our analysis by referring to Fig. 4. As we noted earlier, the mixing efficiency near the cusps is sensitive to variations in flux ratios. Because we want to ensure that the pulse-to-pulse fluctuations in intensities expected in actual systems do not lead to large fluctuations of mixing efficiency, we chose to operate well away from the cusp by using a flux ratio ϕ_3/ϕ_1 of 0.6. For our χ ratio, the theoretical maximum efficiency for infinite cell length at this flux ratio is 23%.

For on-resonance mixing with a single isotope and plane waves, with $N = 2 \times 10^{17}$ cm^{-3}, $L = 100$ cm, and input intensities of $I_1 = 1.22$, $I_2 = 0.76$, and $I_3 = 0.24$ MW/cm^2, our calculations yield an efficiency of 22%, close to the limit of 23%. Similar calculations for Gaussian-spatial-profile beams with the same on-axis intensities predict an efficiency of 16 instead of 22%. The profile of wave four at the exit window is nearly Gaussian, and its phase distortion is negligible. The evolution of the mixing waves looks much like Fig. 2(a), except the saturation length is approximately 20 cm rather than 5 cm. At the end of the 1-nsec square pulse, the maximum 7^1S density occurs at the input window and is 9×10^{13} cm^{-3} or 0.05% of the ground-state atom density. The 7^1S density falls rapidly over the first 10 cm of the cell, similar to the case shown in Fig. 2(b), so the population integrated along the full cell length is approximately 8×10^{14} cm^{-2}. By varying the value of Δk, we find that the width of the index-matching curve (defined as the full width at the points of 67% of maximum efficiency) is 0.65 cm^{-1}.

We now consider whether these results are consistent with limits imposed by parasitic processes. Competing nonlinear processes that could potentially lower these efficiencies include ASE and parametric mixing. The ASE at 1014 nm (7^1S–6^1P) and 407.9 nm (7^1S–6^3P_1) will tend to Rabi split the 7^1S state and thus modify the 6^1S–7^1S two-photon resonance. The effect is to reduce $|S(\Delta_{7S})|$, i.e., the resonant enhancement due to two-photon resonance, and thus reduce the mixing efficiency for a given set of mixing parameters. We have examined this effect experimentally for multiple isotopes and have developed a method for modeling that is described in more detail in Appendix B. Our treatment of ASE is only approximate because we simply replace the Doppler width in Eq. (7) with $(\Delta\omega_D^2 + \omega_{\text{Rabi}}^2)^{1/2}$. This treatment describes the mixing behavior quite well for multiple isotopes and relatively low mixing efficiencies[16] but may be less accurate for high efficiencies. Using this approximation, we compare, in Fig. 11, the mixing efficiency versus Z for two cases: with and without ASE. The conditions are those that produced 22% efficiency above. Inclusion of ASE in our model reduces the efficiency from 22 to 7.5%. Note that the curve with ASE "on" has not saturated even in 100 cm. When Gaussian-spatial-profile input beams are used, the efficiency is 5.0% with ASE on, compared with 16% under the same conditions with ASE turned off.

Clearly ASE has the adverse effect of reducing mixing efficiency. One way to prevent ASE would be to populate the $6P$ levels before the input pulses arrive. From the 6^1S–7^1S population transfer calculated above, we can estimate the $6^{1,3}P_1$ populations needed to prevent ASE and its cost in energy. Because there are three times as many sub-

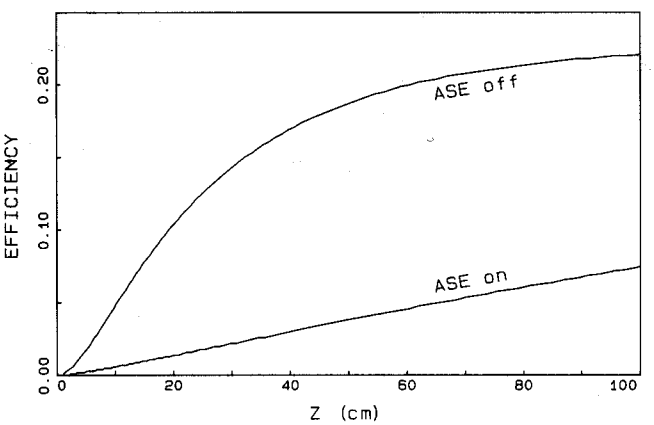

Fig. 11. Efficiency of 130.2-nm generation as a function of position in Hg cell with ASE on and off. Single isotope, $\Delta_{7S} = 0$, $I_1 = 1.2$ MW/cm^2, $I_2 = 0.76$ MW/cm^2, $I_3 = 0.24$ MW/cm^2, $N = 2 \times 10^{17}$ cm^{-3}.

Table 1. Calculated Mixing Efficiencies[a]

Isotopes/6P Prepopulation	On Resonance[b] S/−	S/+	M/−	M/+	Off Resonance M/−	M/+
Intensity (MW/cm^2)						
I_1	1.22	1.22	3.78	3.78	2.7	8.1
I_2	0.76	0.76	2.36	2.36	1.7	5.1
I_3	0.24	0.24	0.74	0.74	1.3	4.0
Efficiency						
Plane wave	7.5	22	11	22	15	62
Gaussian	5.0	16	7.4	16	5	28

[a] $NL = 2 \times 10^{19}$ cm^{-2}; $\omega_{1,2,3} = 255.0, 404.6, 777.2$ nm.
[b] S (M) indicates single (multiple) isotopes; + indicates prepopulated 6P.

levels in each of the two $6P_1$ levels as in the 7^1S level, we would require a population at the input window of 2.7×10^{14} cm^{-3} in each $6P_1$ level. If we integrate along the mixing cell, this equates to a population of at least 2.4×10^{15} cm^{-2} in both $6P_1$ levels. For plane waves, this requires a minimum of 4.5 mJ/cm^2, which would reduce the overall efficiency by a factor of 3. However, if the 6P levels can be populated by using a source of energy cheaper than the mixing waves, this may be attractive. We will not consider methods of populating the 6P levels.

Parametric mixing and changes in index matching due to population transfer and photoionization are both found to make negligible contributions to mixing under the conditions considered here. Detailed analyses are presented in Appendixes B and C.

We summarize our calculations for on-resonance mixing using a single isotope by stating that for plane waves mixing efficiencies are 7.5% with ASE and 22% without ASE, and for Gaussian-spatial-profile waves, efficiencies are reduced to 5 and 16%. These results are listed in Table 1.

2. *Multiple Isotopes*

For on-resonance mixing with multiple isotopes we will assume exact resonance with isotope ^{202}Hg, which is near the maximum of $|S(\Delta_{7S})|$. As may be seen from Fig. 9, the real part of $S(\Delta_{7S})$ is quite small there. This implies that the nonlinear refractive indices will be small at this frequency, and thus the nonresonant isotopes will have little direct influence on the mixing process. The effective density is thus approximately 30% of the total density in proportion to the abundance of ^{202}Hg. More precisely, $|S(\Delta_{7S})|$ is reduced by a factor of 3.1 from 44 to 14 cm. From the scaling relations for mixing efficiency, we expect that in the absence of ASE results close to those for a single isotope can be obtained here by increasing the input intensities by a factor of 3.1. This has been verified numerically for both plane waves and Gaussian-profile beams by comparing curves of efficiency versus Z for single and multiple isotopes. For Gaussian beams, there is a slight (0.25-rad) distortion of the phase front of wave four that is due to the real part of $S(\Delta_{7S})$. The only significant change from the single-isotope case is that the 7^1S population is three times higher because of the greater input intensities.

Again, we must consider whether these results are consistent with potential limiting processes. The principal differences from mixing with a single isotope are the following: (1) the intensities and the population transfer are approximately three times larger and (2) the off-resonance isotopes can support Raman and hyper-Raman gain. We expect that the greater population transfer will still have negligible effect on index matching.

When ASE is included, the $6S$–$7S$ transition is broadened such that all isotopes participate in mixing and ASE. According to our method of including ASE in the modeling of the mixing process, the multiple-isotope case with ASE present looks almost identical to the single-isotope case discussed above. However, prevention of ASE by prepopulating the $6P_1$ levels requires three times the population that is necessary for a single isotope.

Raman and hyper-Raman gain are discussed in Appendix D. Hyper-Raman gain, the off-resonance counterpart of ASE, involves absorption of waves one and two and the emission of a Stokes wave at frequency $\omega_1 + \omega_2 - E_{6P} + E_{7S}$. We show in that appendix that for intensities increased by a factor of 3.1, as discussed above, the off-resonance isotopes support hyper-Raman gain at 1014 nm (7^1S–6^1P), which will interfere with the mixing process. However, this is true only in the absence of ASE. With ASE included, the hyper-Raman gain is greatly reduced and will not affect mixing.

Furthermore, the proposed method of defeating ASE by prepopulating the 6P levels also reduces the hyper-Raman gain below its critical value because of absorption in the wing of the 6^1P–7^1S transition. Note that the hyper-Raman gain coefficient is proportional to the population difference between 6^1S and 6^1P rather than to the population inversion between 7^1S and 6^1P, as for ASE. Thus, although prepopulating the 6^1P level can eliminate the population inversion leading to ASE, it will not significantly reduce the hyper-Raman gain. However, if the absorption in the wing of the 6^1P–7^1S transition is high enough, this gain can be reduced to an acceptable level. The wing absorption is proportional to $N_{6P}{}^2$ because 6^1P_1 atoms broaden the 6^1P_1–7^1S transition far more effectively through resonance broadening than 6^1S ground-state atoms. We show in Appendix D that countering hyper-Raman gain under the conditions of interest here requires a 6^1P density of 1.4×10^{15} cm^{-3} at the input window or <1% of the Hg density. This is comparable with the 6^1P density (1.5% for multiple isotopes) required to prevent ASE. Thus, if ASE is prevented by prepopulating the 6P levels, hyper-Raman gain is also prevented.

The Raman process involves absorption of wave four and emission of a Stokes wave of frequency $(\omega_4 - E_{7S})$. For the nonresonant isotopes the Stokes wave will be shifted from ω_3 and will pump those isotopes from the ground state to 7^1S, depleting wave four. We show in Appendix D that for the mixing conditions considered here ($N = 2 \times 10^{17}$ cm^{-3}, $L =$ 100 cm, $I_1 = 3.78$ MW/cm^2, $I_2 = 2.36$ MW/cm^2, $I_3 = 0.74$ MW/cm^2), the gain is small. Thus the Raman process is insignificant, provided that the mixing lasers have little sideband intensity at the Stokes frequencies.

Our conclusion is that on-resonance mixing using single or multiple isotopes should be capable of generating 130.2-nm light with an efficiency near 10% (see Table 1). The most important efficiency-limiting processes are ASE and hyper-Raman gain. Both can be prevented by prepopulating the $6P_1$ levels in approximately 1% of the Hg atoms at the input window. Ideally, the $6P_1$ prepopulation should follow the 7^1S population and fall off with distance into the mixing cell.

If this can be achieved, mixing efficiencies of 22% for plane waves and 16% for Gaussian beams are predicted. If ASE cannot be avoided, efficiencies fall by approximately a factor of 2.

B. Off-Resonance Mixing

Many of the problems associated with on-resonance mixing can be avoided by tuning a few Doppler widths away from exact resonance. This eliminates significant population transfer and hence ASE. In addition, it removes the restriction to short pulses that would otherwise be imposed to avoid excessive population transfer. It also avoids the efficiency limitations incurred because of interference (see Section 2) so that, in principle, higher efficiencies can be realized off resonance than on resonance.

To avoid ASE it is necessary to detune by approximately 0.5 cm^{-1} for the intensities considered here when using a single isotope. For multiple isotopes, one must detune by slightly less than 0.5 cm^{-1} to the red of the most-abundant isotope. The susceptibilities are nearly the same in either case, so results obtained in one case apply for the other as well. We note that blue detuning for multiple isotopes is not so effective as red detuning because of the presence of the low-abundance mass-196 isotope on the blue side. Avoiding ASE initiated by this isotope requires greater detuning from the abundant isotopes than is necessary for red detuning. Consequently the susceptibility is lower than for red detuning. Although single or multiple isotopes give the same mixing behavior, the competing processes differ and thus will be discussed in the appendixes for each case. We restrict the present discussion to multiple isotopes.

Once again we must be concerned with the pulse-to-pulse variations in intensity expected for actual lasers. We also need to examine the effective width of the index-matching peak. Because of the contributions of the nonlinear phase mismatch Δk_{nl}, the width may be different from that calculated directly from the linear Δk.

We consider first the sensitivity of the mixing efficiency to intensity fluctuations. In Fig. 12 we plot efficiency versus Z, allowing ±15% variations in the intensities of the three plane-wave input beams. The goal here is to pick an operating point that will give stable operation for small fluctuations of input intensities. The dotted curve is for the nominal input intensities, and the other eight curves correspond to conditions whereby each of the three input intensities is independently set to 15% above or below nominal. Δk is set to zero, and the nominal flux ratio is adjusted to compensate for Δk_{nl}. From the set of curves, we can see that if the input intensities can be held to within 15%, consistently high (>60%) efficiency can be achieved, ignoring for the moment other limiting processes.

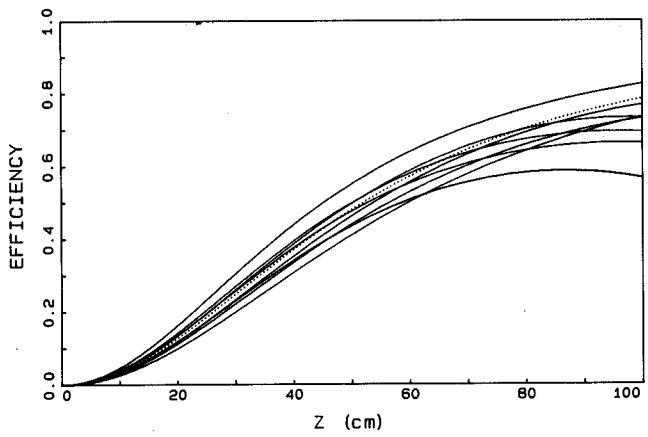

Fig. 12. Sensitivity of off-resonant mixing to variations in input fluxes. $\Delta_{7S} = -0.5$ cm^{-1} ($\omega_1 + \omega_2 = 63\,927.56$), $N = 2 \times 10^{17}$, $I =$ 12.2, 7.68, 6.0 MW/cm^2 for the dotted curve. The other curves are for independent ±15% variations on each intensity.

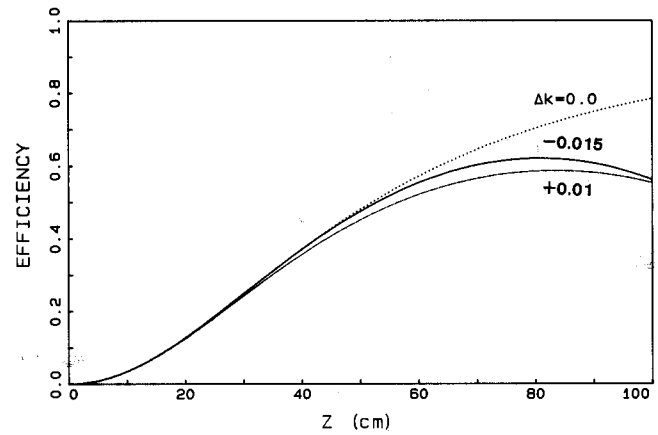

Fig. 13. Same conditions as for dotted curve of Fig. 12 but showing allowable variation in Δk.

If the curve of efficiency versus Z (or equivalently I) were linear, Gaussian-spatial-profile input beams would generate a Gaussian-profile output beam. Hence, for minimal distortion, we should operate in the region where the curves approximate straight lines from the origin. Thus a good operating point from Fig. 12 would be one with $NLIS(\Delta_7)$ corresponding to $Z \leq 70$ cm. Keeping N, L, and the detuning constant, this would correspond to intensities of 8.1, 5.1, and 4.0 MW/cm^2. The calculated efficiency in that case is 62% for plane waves. For Gaussian-profile beams with the same on-axis intensities, the efficiency is 28%, and the profile of the 130.2-nm beam is nearly Gaussian.

Figure 13 gives an indication of the allowable variation in Δk and thus the width of the index-matching peak. The curves describe mixing using plane waves with $\Delta k = 0$, $+0.01$, -0.015 cm^{-1} and the same intensities and density as Fig. 12. From these we conclude that ω_4 can be tuned over approximately 0.5 cm^{-1} here, compared with 0.65 cm^{-1} for on-resonance mixing with no ASE.

Once again we need to consider whether these results are consistent with the limiting processes. Although ASE is avoided by detuning from exact resonance, stimulated Raman and hyper-Raman scattering and parametric gain must still be considered. We show in Appendix D that Raman gain is not important for multiple isotopes, under the mixing conditions discussed above, although the intensity of the 130.2-nm wave is considerably higher than for resonant mixing. However, for a single isotope it could be important because the calculated Raman gain is nearly equal to the estimated critical value for depletion of the 130.2-nm wave. The difference is due to a threefold-larger gain coefficient for a single isotope at the same total density because of the narrower linewidth of the 6^1S–7^1S transition. Thus, if Raman losses are critical, it is clearly preferable to use multiple isotopes.

As was the case for on-resonance mixing, hyper-Raman gain may deplete the mixing waves. As we will discuss in Appendix D, this may be suppressed by a nonlinear interference effect analogous to suppression of population transfer in three-photon-resonant third-harmonic generation. If this does not apply, or if it is not sufficient, prepopulating the 6^1P level to induce wing absorption of the Stokes wave can reduce the gain to an acceptable level. We show in Appendix D that for multiple isotopes, the 6^1P population would need to be approximately 1.6×10^{15} cm^{-3} over the full length of the cell. If neither of these suppression mechanisms is in effect, the hyper-Raman gain can be reduced below its critical value by lowering the intensity of each of the input waves by a factor of 3. Gain suppression by interference or prepopulating the 6^1P level would not affect the mixing efficiencies significantly, whereas lowering the input intensities would reduce efficiencies from 62 to 15% for plane waves and from 28 to 5% for Gaussian-spatial-profile beams. As was the case for Raman gain, the hyper-Raman gain is considerably greater for a single isotope than for multiple isotopes.

We show in Appendix C that for the mixing conditions above (I = 8.1, 5.1, 4.0 MW/cm^2), the parametric process should pose no problems.

To summarize, for off-resonance mixing the single- and multiple-isotope cases give nearly the same behavior for the mixing process. However, the competing Raman and hyper-Raman gains are larger for a single isotope. Thus the use of multiple isotopes is preferred. Loss to the Raman process is not significant for multiple isotopes. Loss to the hyper-Raman process will be significant unless interference or prepopulating the 6^1P level reduces gain or unless the input intensities are lowered by a factor of 3 with a consequent reduction of conversion efficiency. Predicted efficiencies are listed in Table 1.

4. CONCLUSIONS

In Section 2 we discussed optimization of two-photon-(near-) resonant sum-frequency mixing in general. We showed that for exact resonance an interference between waves one and two and waves three and four limits conversion efficiencies. To optimize mixing efficiency it is necessary to adjust the intensities in the three beams to arrive at the best balance between the interference and loss to the mixing medium by two-photon absorption. The optimum balance of intensities depends on the ratio of the partial susceptibilities χ_{12} and χ_{34} associated with the two interfering pathways to the two-photon-resonant level. For χ ratios near unity, efficiencies as great as 35% are possible.

For off-resonant mixing, the interference is not operative, and efficiencies approaching 100% are, in principle, possible. Again, the input intensities must be balanced rather carefully if high efficiency is to be achieved. In this case the intensities are chosen to balance the nonlinear refractive indices for the four waves. For a χ ratio near unity, a good balance can be achieved, resulting in high mixing efficiencies. There is a considerable tolerance in the intensity ratio if Δk is also adjustable and if efficiencies of $\approx$50% are sufficient.

In Section 3 we discussed the specific case of 130.2-nm generation by four-wave mixing in Hg vapor. Our results are summarized in Table 1. We predict efficiencies of the order of 10% in an unfocused and hence energy-scalable geometry using nanosecond-duration pulses. The quality of the output beam is predicted to be near Gaussian for Gaussian-spatial-profile input beams. In making these predictions we have taken into consideration a variety of potential efficiency-limiting processes, including ASE, Raman and hyper-Raman gain, parametric gain, nonlinear refractive indices, two-photon absorption, population transfer, ac-Stark shifts, linear absorption, and isotopic effects.

Our model emphasizes mixing at relatively low intensities and relies on long interaction lengths to achieve high mixing efficiencies. We believe that this permits a realistic treatment of the mixing process. At higher intensities and shorter interaction lengths, the efficiency-robbing processes of hyper-Raman scattering and parametric gain become relatively more important because of the way in which they scale with Hg density, cell length, and input intensities. In addition, the ac-Stark effect introduces time-dependent energy levels. These effects greatly complicate an analysis of mixing at high intensities and may also contribute to the relatively low mixing efficiencies generally reported for sum-frequency mixing using focused beams.

Researchers at Specta Technologies Inc. are currently generating 130-nm light by using the method described here. We plan to collaborate with them in comparing our modeling with their experimental results. In addition, we are continuing to refine our modeling and measurements, especially in developing a more accurate treatment of ASE and also in measuring linear absorption of the mixing waves in Hg vapor.

APPENDIX A: LIMITATIONS ON MERCURY DENSITY, CELL LENGTH, AND INTENSITIES

We consider here upper limits on the Hg density N, the cell length L, and the input intensities I. These are general upper limits. Specific cases may require lower values for I.

We limit the intensities to values lower than those that would result in an ac-Stark shift of the 6^1S–7^1S transition frequency comparable with the Doppler width of approximately 0.067 cm^{-1}. This shift can be calculated reasonably well from the data of Ref. 15. The shifts of the 6^1S and 7^1S states due to each of the four mixing waves are listed in Table 2. They are linear in intensity. For equal photon fluxes in the input beams and with I_3 = 1 MW/cm^2, the 6^1S–7^1S transition frequency shifts by approximately $+2 \times 10^{-3}$ cm^{-1} or 1/25 of the Doppler shift. Thus a reasonable upper limit on the intensities would be 15, 10, and 5 MW/cm^2 for waves 1, 2, and 3, respectively, giving a shift of 0.01 cm^{-1} or 1/7 of the Doppler width.

Table 2. Ac-Stark Shifts of 6^1S and 7^1S Levels of Hg by 1-MW/cm^2 Intensity Light

Frequency (cm^{-1})	Shift of 6^1S (cm^{-1})	Shift of 7^1S (cm^{-1})
39 212 (255.0 nm)	-2.0×10^{-4}	$+9.7 \times 10^{-5}$
24 716 (404.6 nm)	-6.3×10^{-5}	$+3.1 \times 10^{-4}$
12 867 (777.2 nm)	-5.5×10^{-5}	$+1.3 \times 10^{-4}$
76 795 (130.2 nm)	-1.3×10^{-4}	$+7.2 \times 10^{-6}$ [a]

[a] Highly uncertain but probably correct order of magnitude.

At these intensities, photoionization broadening of the 7^1S state should not be a problem. The largest photoionization cross section from 7^1S is for ω_2 because it is resonant with the $6p'[^2D_{3/2}]^1P$ autoionizing state. The peak cross section for this resonance[15] is approximately 2.3×10^{-17} cm^2, so the photoionization broadening at $I_2 = 10$ MW/cm^2 is 0.0024 cm^{-1} or approximately 1/30 of the Doppler width. The corresponding lifetime is 2.2 nsec compared with the radiative lifetime of 31 nsec. The ions and electrons created by photoionization could alter Δk and Stark broaden the Hg levels. This is discussed in Appendix B.

The mixing length is limited in practical applications by the quality of the input light beams. Each beam that deviates from the forward direction by a small angle θ introduces a $\Delta k_{\text{crossing}}$ given by $k\theta^2/2$. If the sum of the contributions from the three input beams is $\geq 1/L$, mixing efficiency will suffer. Thus, for example, if all the input beams were 1 cm in diameter and fives times diffraction limited, this would limit the mixing length to 60 cm. In our modeling we will limit mixing lengths to 100 cm.

The Hg density is limited by the requirements that the width of index matching be large enough to be practical and that linear absorption be acceptably low. The width of index matching is not easily calculated precisely for high mixing efficiency. However, we can estimate the width by calculating the width of the low-efficiency $\text{sinc}^2[\Delta kL/2]$ index-matching curve. For $NL = 2 \times 10^{19}$ cm^{-2}, the width of this index-matching curve[8] for tuning ω_4 is 0.65 cm^{-1} between values of Δk, for which $\text{sinc}^2[\Delta kL/2] = 0.67$. This width is proportional to $(NL)^{-1}$ and must be greater than the laser bandwidths and greater than the Stark shifts of the index-matching peak. The laser bandwidths are assumed to be smaller than the Doppler width of 0.067 cm^{-1}, and Stark shifts of the index-matching point are expected to be comparable with the Stark shift of the 6^1S–7^1S resonance or 0.01 cm^{-1}. Thus, for an acceptable width of the index-matched peak, NL should be kept below 10^{20} cm^{-2}. Thus, for $L = 100$ cm, N should be less than 10^{18} cm^{-3}.

Consideration of linear absorption reduces the maximum allowed Hg density to 2×10^{17} cm^{-3}. Absorption can be due to collisional broadening of the Hg atomic lines and to the presence of Hg dimers, trimers, etc. Consider first wing absorption. Wave one is detuned 200 cm^{-1} to the red of the 6^3P_1 level of Hg and will excite the collisional wing of that level. According to Drullinger *et al.*,[18] the collision-induced absorption coefficient at 255.0 nm is $N^2(3.2 \times 10^{-38})$ cm^{-1}, where N is the Hg density in inverse cubic centimeters. Thus, if wave one is to be attenuated by less than 10% in 100 cm, N must be less than 2×10^{17} cm^{-3}.

The 130.2-nm light will also experience absorption by the collisional red wing of the 8^1P level of Hg. The absorption coefficient has not been measured and cannot be calculated with high confidence. However, we have estimated it by using absorption data for two similar transitions. From the results of Bras and Bousquet[19] for broadening of the $6S$–6^1P transition by Xe, we estimate the absorption coefficient for wave four to be $1.0 \times 10^{-38} N_{\text{Hg}}{}^2$. If instead we use the data of Perrin-Lagarde and Lennuier[20] for broadening of the $6S$–6^3P_1 transition by Hg, the absorption coefficient is 5×10^{-38} $N_{\text{Hg}}{}^2$. At a Hg density of 2×10^{17}, the coefficient is expected to lie between 4×10^{-4} and 2×10^{-3} cm^1. For the higher value, this would result in 20% absorption of the 130.2-nm light over 100 cm for a Hg density of 2×10^{17} cm^{-3}. Because of the uncertainty of these values, we will assume that a density of 2×10^{17} is acceptable.

Wave four at 130.2 nm lies above the ionization threshold energy of Hg_2 and so will be absorbed by Hg dimers. Linn *et al.*[21] present measured relative photoionization curves for Hg and Hg_2. From their data we see that Hg and Hg_2 both have photoionization peaks near 113 nm. The absolute cross section of the Hg peak is known to be $\approx 2 \times 10^{-16}$ cm^2.[22] If we make the assumption that the Hg_2 peak is twice as large, we have a calibration of their relative Hg_2 photoionization cross sections. This calibration fixes the dimer photoionization cross section at 130.2 nm to approximately 1.5×10^{-16} cm^2.

According to Hilpert,[23] the Hg_2 pressure in equilibrium with the Hg atoms is approximated by

$$\frac{[\text{Hg}]^2}{[\text{Hg}_2]} = 1.5 \times 10^9 \exp(-1300/T), \tag{A1}$$

where $[Hg_2]$ and [Hg] are the dimer and atom pressures in pascals and T is the temperature in kelvins. At an atomic density of 2×10^{17} cm^{-3} and a temperature of 200°C, the dimer density is $\approx 2.5 \times 10^{12}$ cm^{-3}. Thus absorption of 130.2-nm light by dimers should be less than 4% over 100 cm.

Absorption of waves two and three is expected to be negligible for densities of a few Torr. Considering the index-match widths and linear absorption, we use 2×10^{17} cm^{-3} as the upper limit on the Hg density.

APPENDIX B: EFFECTS OF POPULATION TRANSFER

1. Amplified Spontaneous Emission

When waves one and two are tuned to two-photon resonance with the 7^1S level, population transfer to the 7^1S level occurs. The result is a population inversion of the 7^1S–$6^{1,3}P$ transitions and gain at the wavelengths 1014 nm (7^1S–6^1P_1) and 407.9 nm (7^1S–6^3P_1). One effect of ASE is to power broaden the 7^1S–6^1P transition with the consequence that the 6^1S–7^1S transition is modified. This ASE process is included in our numerical integration process and can be turned on or off.

Because on-resonance mixing with ASE turned on has been treated in an earlier publication,[16] we will summarize the results here without a detailed discussion of the modeling. When $\omega_1 + \omega_2$ lies within a few Doppler widths of one of the isotopic resonances, population is pumped to the 7^1S level and ASE occurs to lower-lying states. We have studied the effects of population transfer in a difference-frequency mixing experiment. For $\omega_1 = \omega_2 = 312.85$ nm and $\omega_3 = 532$ nm, we generated light at 221.5 nm in a 30-cm column of Hg at 3.5 Torr. We found that for the intensities and Hg densities of these measurements, ASE occurs at 1014 nm, the wavelength of the 7^1S–6^1P transition, but not at 407.9 nm, the wavelength of the 7^1S–6^3P_1 transition. The ASE radiation is strong enough to power broaden the 7^1S–6^1P transition, leading to broadening of the 6^1S–7^1S resonance.

We found that at the relatively low mixing efficiencies ($\approx 10^{-4}$) accessible in our experiments we could model the mixing satisfactorily by replacing the Doppler width of the various isotopic resonances with a power-broadened width

calculated from the ASE intensity at 1014 nm. The ASE intensity in turn is calculated assuming that all atoms pumped to the 7^1S level contribute to the ASE.

One consequence of the ASE broadening is that unsaturated (not limited by the interference effect) mixing efficiency is reduced for a given set of operating conditions because the increased two-photon-resonance linewidth decreases the effective value of $|S(\Delta_{7S})|$. However, the saturated efficiency should still be limited to the same value by the interference effect. It will simply take a considerably larger value of either NL or I to reach a given efficiency than it would have in the absence of ASE.

We also find that according to our method of modeling, there is no noticeable difference between single and multiple isotopes with ASE on because the ASE rapidly broadens the isotopic resonances to widths that are larger than the isotopic shifts.

In the presence of ASE the scaling discussed in Section 2 no longer applies. The plots cannot be applied for other values of $NLI\chi^2$. As a rule, smaller intensities and a larger NL results in lower ASE intensities and better mixing efficiencies.

Another consequence of ASE—one that we have not verified experimentally—is that there may be an increase in bandwidth of the light at the sum frequency. Because the 6^1S–7^1S transition is power broadened by the ASE light, multiple absorption and emission of ASE photons occur in the sum-frequency mixing process. According to the data of Gerstenkorn *et al.*,[24] the bandwidth of the ASE radiation due to isotope and hyperfine splittings is expected to be 0.1 cm^{-1} in the absence of power broadening. Thus we might expect that bandwidth to be added to the bandwidth of the sum-frequency light.

We acknowledge that our modeling of the effects of ASE is rather simplistic and has been verified only in the case of low conversion efficiencies and for a mixture of isotopes. It may be inadequate for high efficiencies or for the treatment of mixing with a single isotope. However, because of the complexity of the process for multiple isotopes for which the 6^1S–7^1S and 7^1S–$6P_1$ both have isotopic structure, a more-accurate model may be difficult to develop. We expect that our model will provide reasonably accurate predictions and will serve to investigate desirable parameter regimes.

2. Population Effects on Index Matching

For both on- and off-resonance mixing we concluded in Section 3 that it is desirable to prepopulate the $6P$ levels with approximately 1% of the ground-state Hg density in order to prevent efficiency loss due to ASE and hyper-Raman gain. In the event that this prepopulation is not achieved, population transfer will still occur for the on-resonance case. In any event, population transfer to 7^1S and the $6P$ states is important, and we must consider its influence on index matching. Ions and electrons produced by photoionization must also be considered.

For there to be an appreciable effect on mixing we must have $\Delta kL \geq 2$. Loss of population in the ground state will not introduce a perturbation in Δk. However, population in the $6P$ and 7^1S levels will. The contribution to Δk due to $7S$ population is difficult to calculate accurately because the sum of ω_1 or ω_2 and $E(7^1S)$ lies in the ionization continuum where it is difficult to calculate Δk. In addition, the contribution of the $6P$ population to Δk cannot be accurately calculated because the relevant oscillator strengths are not known. Instead, we consider the population transfer expected for both on- and off-resonant mixing as discussed in Section 3 and calculate the maximum allowable value of Δk associated with $7S$ and $6P$ atoms. We then discuss whether this condition is likely to be met.

According to the discussion of Section 3, for on-resonance mixing using a single isotope the integrated population transfer to 7^1S is 8×10^{14} cm^{-2}. This implies that a $6P$ ($J = 1$) population of 5×10^{15} cm^{-2} is necessary to avoid ASE. Thus, to keep $\Delta kL < 2$, Δk_{atom} must be less than 2.5×10^{-15} cm^2/atom for 7^1S atoms and 4.0×10^{-16} cm^2/atom for $6P$ ($J = 1$) atoms. From calculations of Δk_{atom} (see Ref. 8), values of 4×10^{-16} and greater will occur only quite close to strong transitions from the level of interest. The principal contributions to Δk that are due to 7^1S population are expected to be due to the states 6^3P_1 [$E(7^1S) - E(6^3P_1) - \omega_2 = -200$ cm^{-1}, $f = 0.002$], $6p'[^2D_{3/2}]^1P$ [$E(6p') - E(7^1S) - \omega_2 = 117$ cm^{-1}, $f = 0.06$], and 8^1P [$E(8^1P) - E(7^1S) - \omega_3 = 68$ cm^{-1}, $f = 0.03$]. Our estimates of Δk_{atom} for the 7^1S atoms is approximately 2×10^{-17} cm^2/atom, well below the maximum allowed value of 2.5×10^{-15} cm^2/atom. In estimating Δk for 6^1P_1 population, we note that no known states lie within 350 cm^{-1} of $E(6^1P_1) \pm (\omega_1, \omega_2, \omega_3, \text{or } \omega_4)$. Thus we expect that Δk due to 6^1P population should be negligible. For 6^3P_1 atoms, Δk should be due primarily to 9^3S [$E(9^3S) - E(6^3P_1) - \omega_1 = -406$ cm^{-1}], 6^1S [$E(6^3P_1) - \omega_1 = 200$ cm^{-1}, $f = 0.024$], and 7^1S [$E(7^1S) - E(6^3P_1) - \omega_2 = -200$ cm^{-1}, $f = 0.002$]. Thus Δk_{atom} for 6^3P_1 atoms is probably smaller than for 7^1S atoms and well below the limit of 4×10^{16} cm^2/atom. These considerations indicate that index matching should not be significantly changed by excited-state populations for on-resonance mixing using a single isotope.

For on-resonance mixing using multiple isotopes the excited-state density must be increased by approximately a factor of 3 relative to that for a single isotope. Again, it is not likely that index matching will be significantly altered.

For off-resonance mixing, approximately 1% of the population may need to be in the 6^1P level over the full length of the cell to prevent hyper-Raman loss. Thus Δk for the 6^1P state must be less than 10^{-17} cm^2/atom. Because calculation of Δk_{atom} is quite uncertain at such low values, it is impossible to state with certainty whether this criterion will be satisfied. However, because there is no population transfer during the mixing pulses and because the prepopulation would be uniform over the full cell length, it should be possible to compensate for any change in Δk due to 6^1P population by readjusting ω_1 and ω_2 slightly.

We have shown that population in the 7^1S and $6P$ ($J = 1$) states should not seriously alter index matching. On the other hand, if a population builds up in the 6^3P_0 metastable state to a level of $>3 \times 10^{15}$ cm^{-2}, it could pose problems because the 6^3P_0–7^3S_1 transition frequency is only 10 cm^{-1} from ω_2 for our proposed mixing scheme. Thus any method of prepopulating the $6P$ levels should avoid populating the 6^3P_0 level.

The contributions of free electrons to Δk must also be considered. For our choice of wavelengths the contribution to Δk from free electrons is approximated by

$$\Delta k_e = +3.7 \times 10^{-17} N_e, \tag{B1}$$

where Δk is in inverse centimeters and N_e is in inverse cubic centimeters. Electrons can be created by photoionization through absorption of wave two by 7^1S atoms or absorption of wave four by ground-state dimers. Assuming on-resonance mixing using a single isotope and taking the worst case of total ionization of all atoms pumped to the 7^1S level, the electron density integrated along the cell length would be approximately 10^{15}. Thus the maximum $\Delta k_e L$ would be 0.04, well below the critical value of two. The free-electron concentration due to dimer ionization would be smaller by a factor of 50 or more. Thus Δk_e is too small to affect the mixing process.

APPENDIX C: PARAMETRIC PROCESSES

Parametric gain processes have been shown to interfere with sum-frequency mixing.[13] The parametric process involves the simultaneous absorption of photons from waves one and two with the emission of two photons at signal and idler frequencies, ω_s and ω_i, where $\omega_s + \omega_i = \omega_1 + \omega_2$ (see Fig. 10). If the index mismatch is not too great, the signal and idler waves can experience exponential growth. The gain will be highest when the signal frequency is nearly resonant with the 7^1S–6^1P transition. This four-wave mixing process can be index matched to the red of the $6P$ resonance if the signal and idler waves propagate at angles relative to the input waves. The exponential gain coefficient for the signal-field amplitude is given by[25]

$$g_s = -\tfrac{1}{2}(k_s'' + k_i'') \pm \tfrac{1}{2}[4G - \Delta k^2 + (k_s'' - k_i'')^2 - 2i\Delta k(k_s'' - k_i'')]^{1/2}, \tag{C1}$$

where k_s'' (k_i'') is the imaginary part of the signal (idler) wave's k vector and Δk is the real part of $k_s + k_i - k_1 - k_2$. The quantity G is defined as

$$G = 7.6 \times 10^{-47}\omega_s\omega_i N^2|S(\Delta_{7S})|^2\,|\chi_{si}|^2 \times |\chi_{12}A_1A_2 + \chi_{34}A_3{}^*A_4|^2, \tag{C2}$$

where ω is in inverse centimeters. χ_{si} is the partial susceptibility for the signal and idler waves and can be evaluated from the plots in Ref. 8. Note that G is proportional to $|\chi_{12}A_1A_2 + \chi_{34}A_3{}^*A_4|^2$, so it has the same z dependence as the 7^1S population. Thus, for $\omega_1 + \omega_2$ tuned on resonance, G exhibits strong interference effects [see Fig. 2(b), for example], whereas off-resonance G is nearly constant with z.

When the absorptions (k_s'', k_i'') and index mismatch (Δk) are zero and the signal frequency is nearly resonant with the 6^1P–6^1S transition, the signal and idler gain coefficients for our case are

$$g_s = G^{1/2} = 8.6 \times 10^{-25}N|S(\Delta_{7S})|\chi_{si}(I_1I_2)^{1/2}. \tag{C3}$$

First we consider parametric gain in the case of a single isotope, no ASE, and on resonance. With $\omega_1 + \omega_2$ tuned to the 7^1S resonance, the signal and idler waves form a third pathway ($\omega_1 + \omega_2$ is one; $\omega_3 + \omega_4$ is a second) from 6^1S to 7^1S. Like waves three and four, these waves can interfere with waves one and two[13] to turn off all two-photon-resonant processes. The parametric process is thus competing directly with the sum-frequency mixing process. The condition for total destructive interference in this case is the same as Eq. (12), i.e.,

$$I_sI_i\,|\chi_{si}|^2 = I_1I_2\,|\chi_{12}|^2. \tag{C4}$$

Because $|\chi_{si}|$ is large near the 6^1P resonance, the product I_sI_i need not be very large to interfere with the sum-frequency mixing process. If the parametric waves reach sufficient intensity to interfere before mixing saturates, the mixing efficiency will suffer. Therefore we consider the growth of the parametric waves in the first 20 cm or so of the mixing cell, for that is approximately the saturation length for the on-resonance mixing discussed in Section 3.

For a single isotope, $|S(0)|$ is 44 cm. We assume for now that k_i'' and Δk are zero. In Table 3 we present calculated values for G, k_s'', and g_s for various detunings of the signal wave from the 6^1S–6^1P transition. G is evaluated at the input window by using our values of χ_{si} (Ref. 8) and setting the value of $\chi_{34}A_3{}^*A_4$ to zero. The k_s'' is calculated from the data of Bousquet and Bras.[26] Note that in the table the gain coefficient g_s is fairly constant over a range of approximately 100 cm^{-1} to the red of the 6^1P level. This is in contrast to the usual observations of parametric gain in a focused beam, in which the gains are highest close to the resonance. From Eq. (C1) one can see that for intensities much higher than we use here, as would be typical in a focused geometry, the gain will be dominated by the $4G$ term that peaks at the resonance. Thus, by using relatively low intensities, we keep the gain low and relatively constant over a broad range.

Table 3. Parametric Gain Evaluation[a]

Δ_{6P}	ω_s	G	k_s''	g_s	I_i^{max}	θ_s (deg)	θ_i (deg)	k_i''
1	54 067.78	600	3700	0.16	9 400	8.0	57	1.5
2	54 066.78	150	920	0.16	9 200	6.3	39	0.81
4	54 064.78	38	230	0.17	9 100	4.7	27	0.51
8	54 060.78	9.7	58	0.17	9 100	3.4	19	0.34
16	54 052.78	2.4	14	0.17	8 750	2.5	14	0.25
32	54 036.78	0.61	3.6	0.16	–	1.8	9.9	0.17
64	54 004.78	0.15	0.9	0.14	–	1.3	6.9	0.12
128	53 940.78	0.038	0.2	0.12	–	0.9	5.0	0.09
256	53 812.78	0.0094	0.06	0.07	–	0.7	3.7	0.07
512	53 556.78	0.0024	0.01	0.04	>16 000	0.6	2.8	0.05

[a] Single isotope, $\Delta_{7S} = 0$, $I_1 = 1.22$ MW/cm^2, $I_2 = 0.76$ MW/cm^2, $N = 2 \times 10^{17}$ cm^{-3}.

Table 3 shows that the gain persists even in the presence of signal absorption larger than G. This is because we assume zero idler loss. Thus the idler grows exponentially, and difference-frequency mixing causes the signal wave also to grow exponentially. When $k_s'' \gg 4G$ and $\Delta k = 0$, one can show that the signal-wave intensity is related to the idler intensity by

$$I_s \approx I_i(\omega_s/\omega_i)(G/k_s''^2). \tag{C5}$$

Thus the condition for destructive interference, Eq. (12), becomes

$$I_i^2 = I_1 I_2 |\chi_{12}|^2/[(\omega_s/\omega_i)(G/k_s''^2)|\chi_{si}|^2]. \tag{C6}$$

The values of I_i that satisfy this condition ($I_1, I_2 = 1.22, 0.76$ MW/cm^2, as in Section 2) are listed in Table 3 as $I_i^{\max}$. Its value is nearly constant at 9×10^3 W/cm^2 for detunings from 1 to 16 cm^{-1}.

At the other extreme, where k_s'' approaches zero (for example, at a detuning of 512 cm^{-1}), I_s is related to I_i by

$$I_i = I_s(\omega_i/\omega_s). \tag{C7}$$

Again, the value of I_i at which interference is total can be calculated from Eq. (C4). For $\Delta = 512$ cm^{-1}, the maximum allowed I_i is 1.6×10^4 W/cm^2. Here Δ is the detuning of the signal frequency from the 6^1P level measured in inverse centimeters. Between $\Delta = 16$ cm^{-1} and 512 cm^{-1}, we expect the value of I_i to increase steadily. Thus the critical value of I_i is rather constant over the same range as the gain, i.e., approximately 100 cm^{-1}. We conclude that the total intensity in the idler wave integrated over the range of 0–100 cm^{-1} to the red of 6^1P must be less than 10^3 W/cm^2 if the efficiency of sum-frequency mixing is to be maintained.

The parametric waves are assumed to build from noise. The appropriate starting value is one half of a photon per mode experiencing gain.[25] To estimate the noise source we need to know the solid angle within which gain occurs. This is derived from the angles θ_s and θ_i for which the various wavelengths index match and from estimates of the allowable deviation from the exact matching angles $\Delta\theta_s$ and $\Delta\theta_i$. These deviations are related to the values of Δk that give zero gain in Eq. (C1). Under our conditions, the gain will be reduced to zero for $\Delta k \geq 80/\Delta$. Thus, for a 1-cm-diameter beam, we estimate the starting noise at approximately 10^{-3} W/cm^2 over the gain bandwidth of 100 cm^{-1}. Because the maximum allowable idler intensity is approximately 10^4 W/cm^2, the parametric power gain must be less than $\approx$15.

From Table 3 the power gain at the input window is 0.32 cm^{-1} for our mixing conditions. Because the parametric gain coefficient is proportional to the 7^1S population, the effective gain length is $\approx$10 cm, implying a total gain of approximately three. Thus it is well below the critical value of 15. At higher input intensities, the parametric gain becomes more important relative to sum-frequency mixing because parametric gain is proportional to I^2, whereas mixing lengths are proportional to I^{-1}. Thus, at higher input intensities, parametric gain can limit mixing efficiencies.

In this analysis we have neglected walk-off losses for the idler wave. Because the idler must propagate at fairly large angles to be index matched, walk off will lead to loss from the idler wave. Assuming that the walk-off loss can be treated as a k_i'' given by

$$k_i'' = (\tan\theta_i)/2D, \tag{C8}$$

where D is the beam diameter, the idler loss is listed in the table for a beam diameter of 1 cm. This loss will lead to lower net gains and will further reduce the importance of parametric gain.

Thus far we have analyzed parametric gain for a single isotope with zero detuning from the two-photon resonance assuming no ASE. We now include ASE and multiple isotopes. For multiple isotopes with no ASE, we showed in Section 3 that the input intensities must be increased by a factor of 3.1 over those for a single isotope in order to achieve the same mixing efficiency. The increase is necessary to compensate the reduction of 3.1 in $S(\Delta_{7S})$. Because G and hence g_s (for $k_s'' \gg G$) is proportional to $[IS(\Delta_{7S})]^2$, with this increased intensity the parametric gain for multiple isotopes should be the same as it was for a single isotope. Similarly, the inclusion of ASE involves a reduction of $S(\Delta_{7S})$. Because parametric gain is proportional to $|S(\Delta_{7S})|^2$, it is expected to be negligible in the presence of ASE as well.

The analysis of parametric gain off resonance is similar to the on-resonance analysis. Higher signal and idler intensities (and hence gains) are permitted because it is pump depletion rather than interference that sets the allowable limits. Thus the maximum allowable gain is increased from 15 on resonance to 20 off resonance. In addition, the parametric gain is nearly constant over the full length of the Hg cell, for interference does not lead to reduction of the gain coefficient. If we use the intensities ($I_1, I_2, I_3 = 8.1, 5.1, 4$ MW/cm^2) and the detunings suggested in Section 3 for off-resonance mixing with multiple isotopes, G is reduced by a factor of 14 from those of Table 2. Near the 6^1P resonance, where $k_s'' \gg (4G)^{1/2}$, g_s will be reduced by the same factor of 14, whereas farther from resonance, where k_s'' is small, g_s will be reduced by a factor of $14^{1/2}$. Thus near the 6^1P resonance the power gain is $0.32/14 = 0.023$ cm^{-1}, so over the full length of the mixing cell the gain is only 2.3, well below the critical value of 20. Thus we expect that parametric gain should pose no problem for off-resonance mixing.

APPENDIX D: RAMAN AND HYPER-RAMAN SCATTERING

Stimulated Raman and hyper-Raman scattering (Fig. 10) are potential loss mechanisms for off-resonance mixing and for on-resonance mixing with multiple isotopes. The Raman process creates loss for 130.2-nm light and gain for Stokes light at $(\omega_3 + \Delta_{7S})$. If the Raman gain is high enough, a Stokes wave can build up at the expense of the 130.2-nm wave. The hyper-Raman process involves absorption of waves one and two and the emission of photons of energy $E_{7S} - E_{6P} + \Delta_{7S}$. For sufficiently high gain this will deplete waves one and two and thus reduce the mixing efficiency. Both of these processes result in the exponential gain of a Stokes wave that, in the absence of other applied source light, has an initial or source intensity of one photon per gain mode.

1. Raman Process

Assuming a beam diameter of 1 cm and a cell length of 100 cm, the Stokes source intensity[25] for the Raman process is estimated as $\approx 10^{-5}$ W/cm^2

The Raman gain exponent is calculated using[25]

$$g_{\text{Raman}} = 8.77 \times 10^{-25} \omega_{\text{Stokes}} S''(\Delta_{7S}) N \langle I_4 \rangle |\chi_{34}|^2, \quad \text{(D1)}$$

where $\langle I_4 \rangle$ is I_4 in W/cm^2 averaged over the length of the Hg cell, ω_{Stokes} is $(\omega_3 + \Delta_{7S})$ in inverse centimeters and $S''(\Delta_{7S})$ is the imaginary part of $S(\Delta_{7S})$.

For on-resonance mixing with multiple isotopes, the isotopes with mass different from 202 will be detuned and can support Raman gain. For this case the 130.2-nm beam reaches an intensity of 1.5 MW/cm^2, according to the modeling discussed in Section 3. Thus for a 10% loss to the 130.2-nm wave due to Raman gain, the Stokes wave must build to an intensity of 2.5×10^4 W/cm^2. This implies a critical gain exponent of 22. Using Eq. (D1), we obtain for the calculated gain exponent for this case a value of 1.5, which is well below the critical value.

For off-resonance mixing with multiple isotopes (discussed in Section 3), $\langle I_4 \rangle$ is higher by a factor of 4. However, the Raman gain is still expected to be below the critical value. In contrast, for off-resonance mixing with a single isotope, $S''(\Delta_{7S})$ is also increased by a factor of 3, and the calculated gain exponent of 24 would be near the critical value. Thus we should be below Raman threshold for off-resonance mixing using multiple isotopes but perhaps not for off-resonance mixing using a single isotope.

In this discussion we have assumed that the source of Stokes light was the zero-point vacuum noise. If there is significant sideband light in wave three at the Stokes frequency, the critical gain exponents could be considerably lower. In fact, the calculated gains imply that the sideband light at the Stokes frequency must be less than approximately 500 (3×10^4) W/cm^2 cm^{-1} for off- (on-) resonance mixing using multiple isotopes.

We have assumed that the Raman processes pump the 7^1S state. Raman processes pumping the 7^3S or 6^1D states are also energetically allowed. However, the values of χ_{34} for the 7^3S is much smaller than for 7^1S, so we can safely ignore this possibility. The gain for the 6^1D cannot be calculated with accuracy because the P–D oscillator strengths are not known. Our best estimate of the gain exponent for this process is based on the calculated oscillator strengths of Hafner and Schwarz[27] and is about one tenth that of the $6S$–$7S$ gain; thus this is also insignificant.

2. Hyper-Raman Process

Hyper-Raman gain is a potential loss mechanism for both on-resonance mixing using multiple isotopes and off-resonance mixing. The gain coefficient is calculated using[25]

$$g_{\text{hyper-Raman}} = 4.3 \times 10^{-13} \omega_{\text{Stokes}} |d_{7S-6P}|^2 N S''(\Delta_{6P}) S(\Delta_{7S})^2 \times |\chi_{12} A_1 A_2 + \chi_{34} A_3^* A_4|^2, \quad \text{(D2)}$$

where d_{7S-6P} is the dipole-transition matrix element for the 7^1S–6^1P transition expressed in units of ea_0. The gain coefficient at the input window is given by

$$g_{\text{hyper-Raman}} = 3.83 \times 10^{-33} N I_1 I_2 S''(\Delta_{6P})\, S(\Delta)^2, \quad \text{(D3)}$$

where $S''(\Delta_{6P})$ is the imaginary part of the line-shape function for the Doppler-averaged 6^1S–6^1P transition, I is in watts per square centimeter, ω_{Stokes} is the Stokes frequency in inverse centimeters.

We first consider on-resonance mixing. The maximum allowed Stokes intensity is approximately 10^4 W/cm^2, for at this intensity saturation of the 6^1P_1–7^1S transition by Stokes light will power broaden the 7^1S level and thus affect sum-frequency mixing. Thus, with a noise source of 10^{-6} W/cm^2, the critical value for the gain exponent is approximately 23. The calculated hyper-Raman gain coefficient for off-resonant isotopes at the input window ($N = 2 \times 10^{17}$, $I_1 = 3.8$, $I_2 = 2.4$ MW/cm^2) is 4.5 cm^{-1}. Over the effective mixing length of 10 cm, the value of $g_{\text{hyper-Raman}} L_{\text{effective}}$ is 45, clearly exceeding the critical value.

Because the hyper-Raman gain coefficient is proportional to NI^2, whereas the effective gain length (set by the mixing length) is proportional to $(NI)^{-1}$, one way to reduce the hyper-Raman gain is to reduce I by a factor of 3 or so. This would reduce $g_{\text{hyper-Raman}} L_{\text{effective}}$ by three to 15, which is below the critical value.

Another way to reduce the gain is to prepopulate the 6^1P level and rely on wing absorption of the 6^1P–7^1S transition to counteract the gain. For the necessary absorption coefficient of 3 cm^{-1} for a detuning comparable with the isotope shift of 0.3 cm^{-1}, this would require a 6^1P population of approximately 1.4×10^{15} cm^{-3} or <1% of the total Hg density. This would be the density at the input window, and the density could fall to zero in 15 cm or so.

We now turn to off-resonance mixing. Here the critical value of the gain exponent is set by loss of light from the mixing beams and is approximately 26. For the highest intensities considered in Section 3 for off-resonance mixing with multiple isotopes (I = 8.1, 5.1, 4.0 MW/cm^2), the gain-calculated hyper-Raman gain coefficient is 1.5 cm^{-1}. If the gain is nearly constant over the full length of the cell, this is unacceptable. As in the case of on-resonance mixing, this can be lowered to a tolerable value by reducing the input intensities by three.

Alternatively, loss can be introduced by populating the 6^1P level at a density of 1.6×10^{15} cm^{-3} over the full length of the cell.

It seems possible that the hyper-Raman Stokes wave could mix with waves one and two to generate difference-frequency light resonant with the 6^1S–6^1P transition. In analogy with three-photon-resonant third-harmonic generation[14] this could set up a destructive interference that prevents population transfer to the 6^1P state. This would suppress hyper-Raman gain in the forward direction but not in the backward direction because index matching is approximately satisfied only in the forward direction. If this occurs the effective gain length is not 100 cm, as assumed above, but rather it is one half the pump-pulse length or 15 cm. This effect may make it unnecessary to prepopulate the 6^1P level or to reduce the input intensities, for the value of $g_{\text{hyper-Raman}} L_{\text{effective}}$ is only 22. For on-resonance mixing the effective length is set by the mixing length at 10 cm, so this interference would not reduce the overall gain much in that case.

ACKNOWLEDGMENTS

We thank Peter Esherick for carefully reading the manuscript and suggesting many improvements. This research was performed at Sandia National Laboratories and was supported by the U.S. Department of Energy under contract DE-AC04-76DP00789 for the Office of Basic Energy Sciences, Division of Chemical Sciences.

REFERENCES

1. H. F. Dobele, M. Rowekamp, and B. Ruckle, "Amplification of 193 nm radiation in argon-fluoride and generation of tunable VUV radiation by high-order anti-Stokes Raman scattering," IEEE J. Quantum Electron. **QE-20,** 1284–1287 (1984).
2. W. Jamroz, P. E. LaRocque, and B. P. Stoicheff, "Generation of continuously tunable coherent vacuum-ultraviolet radiation (140–106 nm) in zinc vapor," Opt. Lett. **12,** 617–619 (1982).
3. T. J. McKee, B. P. Stoicheff, and S. C. Wallace, "Tunable, coherent radiation in the Lyman-α region (1210–1290 Å) using magnesium vapor," Opt. Lett. **3,** 207–208 (1978).
4. R. Hilbig and R. Wallenstein, "Resonant sum and difference frequency mixing in Hg," IEEE J. Quantum Electron. **QE-19,** 1759–1770 (1983).
5. K. Miyazaki, H. Sakai, and T. Sato, "Coherent VUV generation by resonantly-enhanced nonlinear frequency mixing in Cd vapor," IEEE J. Quantum Electron. **QE-22,** 2266–2271 (1986).
6. D. M. Bloom, G. W. Bekkers, J. F. Young, and S. E. Harris, "Third harmonic generation in phase-matched alkali metal vapors," Appl. Phys. Lett. **26,** 687–689 (1975); H. Puell, K. Spanner, W. Falkenstein, W. Kaiser, and C. R. Vidal, "Third-harmonic generation of mode-locked Nd:glass laser pulses in phase-matched Rb–Xe mixtures," Phys. Rev. A **14,** 2240–2257 (1976); K. N. Drabovich, D. I. Metchkov, V. M. Mitev, L. I. Pavlov, and K. V. Stamenov, "Tunable resonant third harmonic generation of picosecond pulses in sodium vapour," Opt. Commun. **20,** 350–353 (1977); M. H. R. Hutchinson and R. J. Manning, "Efficient generation of high-power VUV ultrashort pulses by four-wave mixing," Opt. Commun. **55,** 55–60 (1985).
7. R. Mahon and F. S. Tomkins, "Frequency up-conversion to the VUV in Hg vapor," IEEE J. Quantum Electron. **QE-18,** 913–920 (1982).
8. A. V. Smith and W. J. Alford, "A practical guide for 7*S* resonant mixing in Hg: generation of light in the 230–185 and 140–120 nm ranges," submitted to J. Opt. Soc. Am. B.
9. H. Kildal and S. R. J. Brueck, "Pump depletion and saturation of two-photon resonant third-harmonic generation processes," IEEE J. Quantum Electron. **QE-16,** 566–573 (1980).
10. J. F. Reintjes, *Nonlinear Optical Parametric Processes in Liquids and Gases* (Academic, New York, 1984).
11. B. D. Fried and S. D. Conte, *The Plasma Dispersion Function* (Academic, New York, 1961).
12. R. D. Richtmyer and K. W. Morten, *Difference Methods for Initial-Value Problems,* 2nd ed. (Wiley-Interscience, New York, 1967), p. 199.
13. R. W. Boyd, M. S. Malcuit, and D. J. Gauthier, "Competition between amplified spontaneous emission and the four-wave-mixing process," Phys. Rev. A **35,** 1648–1658 (1987); V. I. Anikin, V. D. Gora, K. N. Drabovich, and A. N. Dubovik, "Theory of frequency addition under resonance conditions," Sov. J. Quantum Electron. **6,** 174–178 (1976); E. A. Manykin and A. M. Afanas'ev, "Resonance phenomena in nonlinear optics," Sov. Phys. JETP **21,** 619–623 (1965).
14. M. G. Payne and W. R. Garrett, "Theory of the effect of third-harmonic generation on three-photon resonantly enhanced multiphoton ionization in focused beams," Phys. Rev. A **28,** 3409–3429 (1983); J. J. Wynne, "Polarization renormalization due to nonlinear optical generation," Phys. Rev. Lett. **52,** 751–754 (1984).
15. A. V. Smith and W. J. Alford, "Vacuum ultraviolet oscillator strengths of Hg measured by sum-frequency mixing," Phys. Rev. A **33,** 3172–3180 (1986); W. J. Alford and A. V. Smith, "Measured third-order susceptibility and excited state oscillator strengths for atomic mercury," Phys. Rev. A **36,** 641–648 (1987).
16. A. V. Smith, G. R. Hadley, P. Esherick, and W. J. Alford, "Efficient two-photon-resonant frequency conversion in Hg: the effects of amplified spontaneous emission," submitted to Opt. Lett.
17. Oak Ridge National Laboratory, *Catalog of Isotopes Products and Services* (Oak Ridge National Laboratory, Oak Ridge, Tenn., 1983).
18. R. E. Drullinger, M. M. Hessel, and E. W. Smith, "Experimental studies of mercury molecules," J. Chem. Phys. **66,** 5656–5666 (1977).
19. N. Bras and C. Bousquet, "Spectre d'absorption de la raie 1849 Å du mercure élargie élargie par effet de pression des divers gaz rares. Determination des potentiels d'interaction Hg–Xe," J. Phys. **40,** 945–960 (1979).
20. D. Perrin-Lagarde and R. Lennuier, "Mesure experimentale du coefficient d'absorption de la vapeur de mercure dans la région de la raie de resonance λ = 2537 Å," C. R. Acad. Sci. Paris **274,** 1020–1023 (1972).
21. S. H. Linn, C. L. Liao, C. X. Liao, J. M. Brom, Jr., and C. Y. Ng, "Photoionization study of Hg_2," Chem. Phys. Lett. **105,** 645–650 (1984).
22. R. Lincke and B. Stredele, "Absorptionsquerschnitt und Oszillatorenstärke der autoionisierenden Linie Hg I 1126,6 A," Z. Phys. **238,** 164–171 (1970).
23. K. Hilpert, "Mass spectrometric equilibrium study of the molecule Hg_2," J. Chem. Phys. **77,** 1425–1427 (1982).
24. S. Gerstenkorn, J. J. Labarthe, and J. Vergès, "Fine and hyperfine structures and isotope shifts in the arc spectrum of mercury," Phys. Scr. **15,** 167–172 (1977).
25. D. C. Hanna, M. A. Yuratich, and D. Cotter, *Nonlinear Optics of Free Atoms and Molecules* (Springer-Verlag, New York, 1979).
26. C. Bousquet and N. Bras, "Profil de la raie 1849 Å du mercure autoelargie par effet de pression. Determination des potentiels d'interaction Hg–Hg," J. Phys. **41,** 19–29 (1980).
27. P. Hafner and W. H. E. Schwarz, "Atomic transition probabilities from relativistic pseudopotential approach," J. Phys. B **11,** 2975–2999 (1978).